Determination of Melanoma Lateral and Depth Margins: Potential for Treatment Planning and Five-Year Survival Rate

Tianyi Wang, Jinze Qiu and Thomas E. Milner
The University of Texas at Austin
USA

1. Introduction

Cutaneous malignant melanoma (CMM) is a serious type of cancer accounting for 75% of all deaths associated with skin cancer (Jerant et al., 2000). CMM incidence has dramatically increased in the past few decades and, recently, approximately 160,000 new cases of CMMs are diagnosed worldwide each year (Ries et al., 2003). In 2010, the American Cancer Society estimated that 68,130 cases of melanoma (38,870 males; 29,260 females) and 8,700 melanoma deaths (5,670 males; 3,030 females) were expected in the United States (American Cancer Society (ACS), 2010). In the United States, the lifetime risk for developing CMM has increased from 1 in 1500 in 1930 to 1 in 50 in 2010 (ACS, 2010; King, 2004).

Proper staging of CMM is crucial for defining prognosis and for determining the optimal treatment approach. Several cancer staging systems are being used worldwide. One of the most common staging systems is the tumor-node-metastasis (TNM) classification established by the American Joint Committee on Cancer (AJCC) (Balch et al., 2001). The TNM system classifies CMM in three categories: (1) the size and extent of the primary tumor (T), (2) the involvement of regional lymph nodes (N) and, (3) the presence or absence of distant metastasis (M), determining CMM clinical Stage I, II, III, or IV. To remain current and relevant to clinical practice, the TNM classification is updated periodically based on advances in understanding of cancer prognosis. The latest revision of TNM (presented in the 7th edition of the AJCC Cancer Staging Manual) is applied for cases diagnosed on or after January 1, 2010 (Edge et al., 2010). The CMM invasion depth known as the Breslow thickness (Breslow, 1970) in T category is the single most important factor for CMM staging and closely related to survival rate (Mihm et al., 1988). The five-year survival rate is 95%-100% if CMM thickness is less than 1 mm, while the survival rate is reduced to 50% if the tumor thickness is greater than 4 mm (Figure 1).

Current surgical treatment for primary CMM has often been an excision with a margin determined by CMM thickness (Table 1). Since the risk of local recurrence is dependent on CMM thickness, a narrow margin of 5 mm is recommended for *in situ* CMMs, 1 cm for tumors thinner than 1 mm, 1-2 cm for tumors between 1.01 and 2 mm, and 2 cm for tumors thicker than 2.01 mm (Sladden et al., 2009). Because sentinel lymph node highly correlates with the metastatic status of CMM, a sentinel lymph node dissection (SLND) procedure is also performed on patients with intermediate thickness (1-4 mm) lesions (Balch & Ross,

1999; Kanzler & Mraz-Gernhard, 2001). Therefore, detection of CMM thickness is clinically significant and essential for five-year survival rate and surgical margin determination.
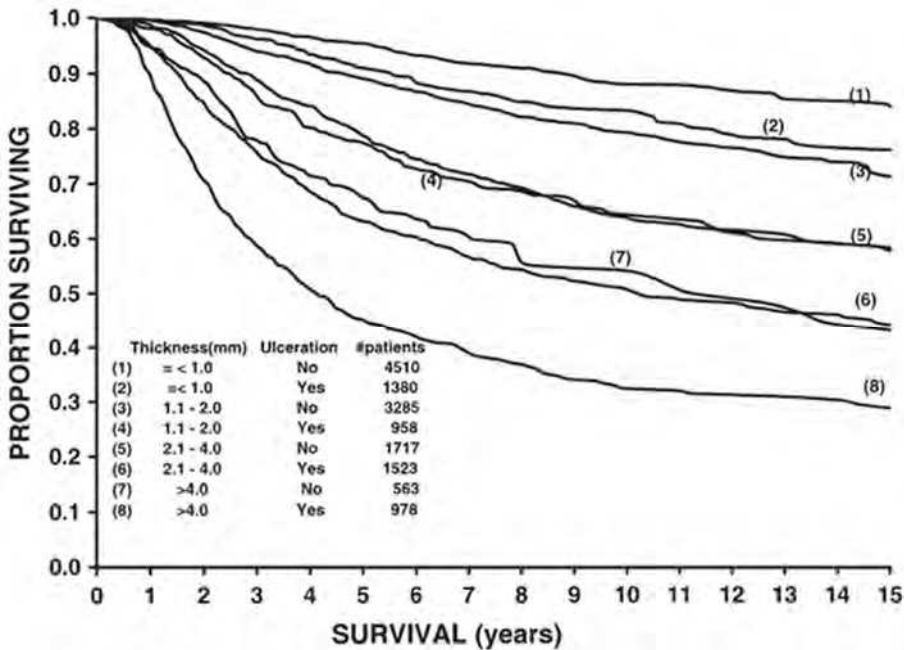

Fig. 1. CMM thickness and survival rate. Image adopted from Rubin., 2010.

T Category Classification	Breslow Thickness (mm)	Ulceration Status /Mitoses	Excision Margin (cm)
TX		Primary tumor cannot be assessed	
T0		No evidence of primary tumor	
Tis		Melanoma *in situ*	0.5
T1	≤ 1.0	Without ulceration or mitosis < 1 mm²	1
		With ulceration or mitosis > 1 mm²	
T2	1.01-2.0	Without ulceration	1-2
		With ulceration	
T3	2.01-4.0	Without ulceration	2
		With ulceration	
T4	> 4.0	Without ulceration	2
		With ulceration	

Table 1. CMM classification in T category and current U.S. guidelines for excision margins.

The current gold standard for CMM diagnosis and tumor thickness measurement is achieved by taking a small biopsy for standard histology (Gambichler et al., 2006). Biopsy and histology allows the visualization of structures in a vertical section of the skin (i.e., from

the epidermis through to the reticular dermis or even subcutaneous tissue). However, this procedure is invasive, time consuming and the sensitivity/specificity of CMM detection is highly dependent on location of biopsy. A real clinical need is recognized for non-invasive imaging techniques for *in vivo* evaluation of CMM. Currently, magnetic resonance imaging (MRI), computed tomography (CT), positron emission tomography (PET), high-frequency ultrasound (HFUS), optical coherence tomography (OCT), photoacoustic imaging (PAI), pulsed photothermal radiometry (PPTR), scanning confocal microscopy (SCM), multi-photon luminescence microscopy (MPLM), second harmonic generation (SHG), dermoscopy, multispectral imaging (MSI), diffuse reflectance spectroscopy (DRS) and Raman spectroscopy (RS) or some combination of these are being investigated for non-invasive diagnosis of CMM. Although MRI, CT and PET have the ability to identify nodal and distant metastasis, their routine use for localized CMM investigation is not indicated due to insufficient spatial resolution (King, 2004). Dermoscopy, MSI, DRS and RS are able to identify intrinsic differences between CMM, dysplastic nevi and normal skin but without providing the depth profile of CMM. SCM, MPLM and SHG provide the highest spatial resolution among all these imaging techniques and can also identify the morphological differences in CMM compared with dysplastic nevi. Moreover, SCM, MPLM and SHG have been successfully used to preoperatively delineate CMM lateral margins. However, the penetration depth of SCM, MPLM and SHG limits their use to detect depth margins of intermediate (1-4 mm) and more advanced (>4 mm) CMMs. HFUS, OCT, PAI and PPTR have spatial resolutions and penetration depths between MRI/CT/PET and SCM/MPLM/SHG, which underlines their potential applicability to not only diagnose CMM but also to detect lateral and depth margins.

This chapter examines the evidence for use of non-invasive imaging techniques, in particular, MRI, CT, PET, HFUS, OCT, PAI, PPTR, SCM, MPLM and SHG, in CMM diagnosis as well as tumor lateral and depth margin detection for preoperative CMM staging and surgical margin definition. Comparison between these imaging techniques in terms of spatial resolution, penetration depth, sensitivity/specificity, correlation with histology and temporal monitoring (possibility to monitor CMM changes at multiple time points) are described and, recommendations for future studies are indicated.

2. CMM imaging techniques

2.1 Magnetic Resonance Imaging (MRI)

Atomic nuclei in a magnetic field oscillate in the direction of the field at a specific frequency directly related to the field strength and the magnetic properties of the nuclei. If a pulse of current of the same frequency is applied to the coil surrounding the nuclei, an oscillating magnetic field is produced that creates a radio frequency within the coil. Magnetic field energy is absorbed by the nuclei and re-emitted as a radio-frequency signal immediately after the applied pulse. The re-emitted radio frequency energy is measured by the surface coil and reconstructed to form an MRI image (Baddeley, 1984). MRI has been widely employed in clinical oncology and introduced to examine cutaneous melanocytic and other types of skin lesions since 1989 (Zemtsov et al., 1989) due to good contrast between tumor regions and soft tissues (Totty et al., 1986; Weeks et al., 1985). The application of MRI to dermatology has become practical with the development and application of specialized surface coils that allow higher resolution imaging than standard MRI coils (Bittoun et al., 1990; Hyde et al., 1987; Marghoob et al., 2003; Querleux et al., 1988, 1995; Rajeswari et al.,

2003; Richard et al., 1991; Zemtsov et al., 1989). Although imaging thin cutaneous tumors (i.e., <1 mm) is not possible due to insufficient resolution, MRI was utilized to evaluate advanced skin tumors, particularly to determine the depth of malignant tumors and the degree of invasion. el Gammal et al combined a strong homogeneous magnetic field of 9.4 T with gradient fields of 11.7 G/cm and an imaging unit to obtain a voxel resolution of $40\times40\times300$ µm^3, allowing differentiation between normal skin and skin tumors including CMMs (Figure 2) (el Gammal et al., 1996). Using this approach, a primary nodular melanoma with Breslow thickness of 1.65 mm was imaged. The tumor is visible in the image (Figure 2d) in the upper left part of the histological section. Skin layer, sub-layers and tumor were visualized by MRI (Figure 2c) with different signal contrast. An excellent correlation between MRI image and corresponding histological features was achieved.
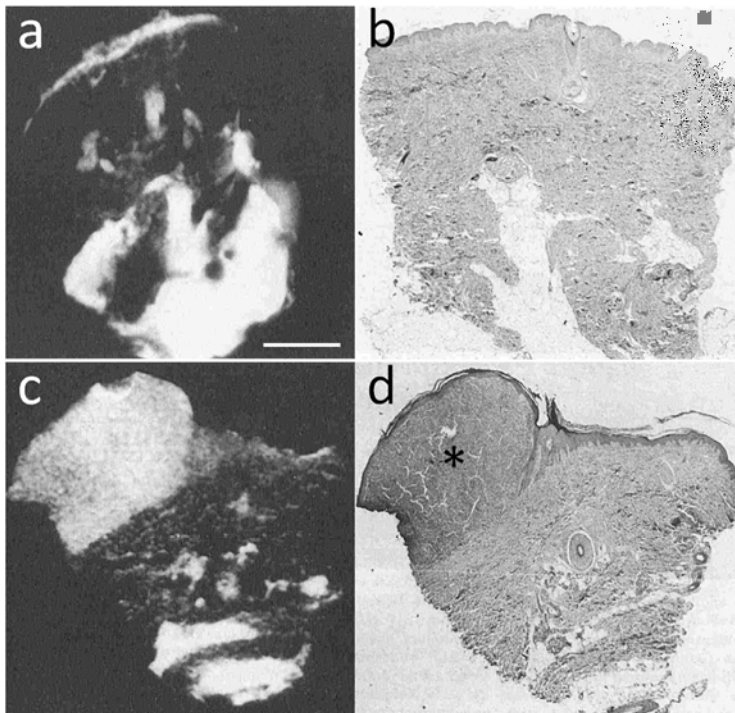

Fig. 2. (a,b) MRI and corresponding histology images, respectively, of normal skin from the upper leg of a 25-year-old man. (c,d) MRI and corresponding histology images, respectively, of primary nodular melanoma from the leg of a 31-year-old woman. (*) indicates the tumor location in (d) . Breslow thickness of the tumor was 1.65 mm. Scale bar is 1 mm. Image modified from el Gammal et al., 1996.

Ono et al applied MRI to the diagnosis of malignant skin tumors and reported selected cases (Ono & Kaneko, 1995). A more advanced CMM with lateral dimensions of 36×26 mm^2 was imaged (Figure 3). The MRI image (Figure 3a) was found to reflect precisely the actual morphology and tumor depth (Figure 3b). The reconstructed 3-D MRI image (Figure 3c) yielded accurate information regarding the relationship between tumor and its surrounding

Determination of Melanoma Lateral and Depth Margins:
Potential for Treatment Planning and Five-Year Survival Rate
113

tissue and also provided a 3-D view of the state of infiltration, useful for deciding on a resection area prior to surgery. MRI has also been used to image nodal and distant metastasis in a murine model (Foster et al., 2008) as well as different organs in humans (King, 2004). However, the availability and cost of MRI is a limiting factor. Therefore, although MRI is useful for advanced CMM thickness measurement and individual metastasis characterization, at present this approach is not a first-line investigation tool.
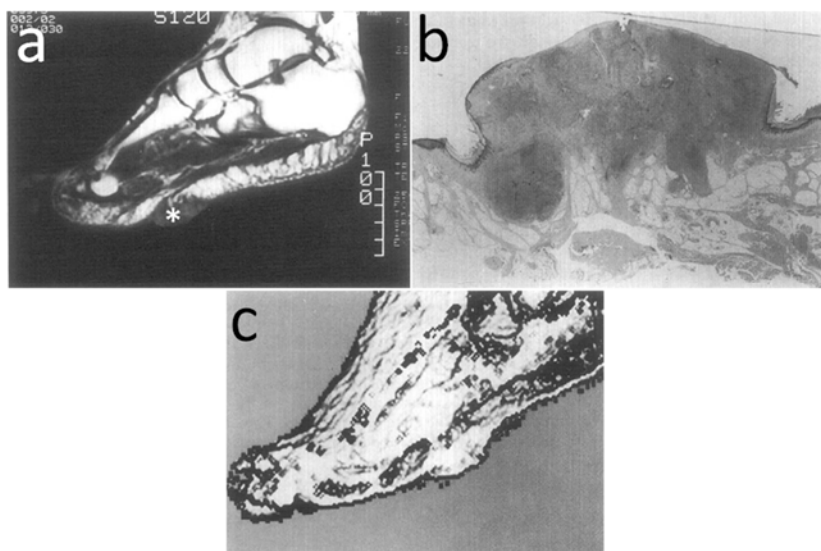

Fig. 3. CMM on the left sole of a 67-year-old woman. (a) MRI image longitudinally sectioning the tumor demonstrated an irregularly convex and concave region at the thick base of the tumor. (b) Histological section of the tumor. (c) A reconstructed 3-D image prepared from MRI slices. (*) indicates the tumor location in (a). Image modified from Ono & Kaneko, 1995.

2.2 Computed Tomography (CT) and Positron Emission Tomography (PET)

CT produces images with contrast given by the attenuation of X-ray photons by differing body tissues, in a manner similar to conventional radiography (Baddeley, 1984). Because CT has comparable or lower resolution than MRI (Link et al., 2003), it is not indicated to diagnose patients with primary CMMs but rather metastasis. The identification of CMM metastasis is dependent on the morphologic alteration of tissue malignancy and, therefore, CT is insensitive at detecting small tumor masses. Chest CT is sensitive to detect nodules (<1 cm), calcification within a nodule and to distinguish solitary from multiple pulmonary lesions (Armstrong et al., 2001; Halton, 1992). Although these findings are often non-specific for malignancy, they can provide a baseline scan allowing serial assessment of changes. Heaston et al showed that chest CT detected CMM metastasis in 19% of patients with normal chest X-ray (Heaston et al., 1983).

PET, a whole-body imaging technique, is widely used in the diagnosis of metastatic cancer. In a PET imaging procedure, an isotopic tracer is injected and used to label cancer cells.

Fluoro-deoxy-glucose (FDG) is one of the most widely applied PET tracers used to survey cell metabolism (Gritters et al., 1993; Strobel et al., 2007; Wagner et al., 1999). Because metabolic characterization of tumor cells usually exceeds physiological metabolic activity, excessive FDG uptake has consequently been demonstrated in most cancers *in vivo*, making whole-body FDG-PET a sensitive indicator of metastatic CMM compared with conventional diagnostic imaging modalities (Blessing et al., 1995; Boni et al., 1995; Damian et al., 1996; Gritters et al., 1993; Macfarlane et al., 1998; Rinne et al., 1998; Steinert et al., 1995; Wagner et al., 1997). The improved sensitivity and potential cost-effectiveness of FDG-PET are rational arguments for PET staging of patients with recurrent CMM (Yao et al., 1994). The sensitivity of PET depends on the location and size of the tumor. A resolution of 4-6 mm is usual, which suggests that PET may lack the sensitivity to detect small nodular CMM metastasis that are usually 1-2 mm in size (Belhocine et al., 2006).

As PET alone does not provide sufficient resolution to detect small CMM metastasis, it is usually used in combination with CT (Akcali et al., 2007; Essner et al., 2006), allowing mapping of PET images onto CT images acquired simultaneously (Figure 4). Reinhardt et al studied 251 patients with PET/CT and showed a sensitivity of 98.7% compared to 88.8% for PET alone and 69.7% for CT alone (Reinhardt et al., 2006). Moreover, Iagaru et al recently reported a study involving 163 patients and showed a sensitivity of 89%, and recommended the use of PET/CT in the evaluation of high-risk CMM metastasis (Iagaru et al., 2006).
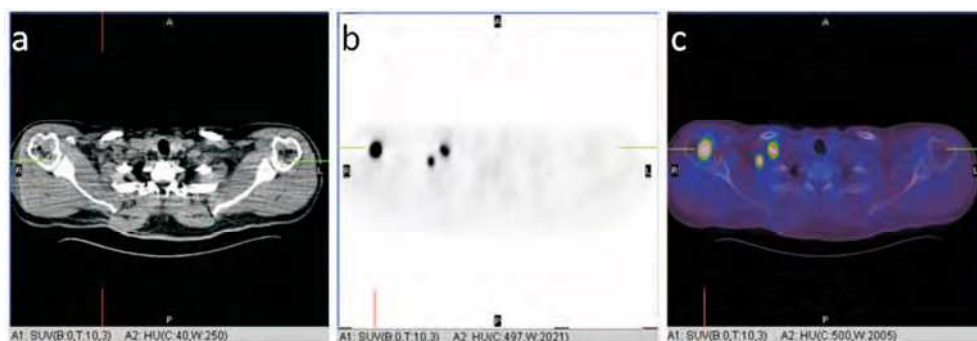

Fig. 4. ^{18}F-fluorodeoxyglucose PET/CT for restaging of a 56-year-old patient with a superficial spreading melanoma of 4.3 mm depth at the right shoulder after resection of a lymph-node metastasis at the right neck. (a) CT, (b) PET and (c) fused PET/CT images showed two lymph-node metastasis infraclavicular, and PET showed an additional metastasis that was found to be localized in the right humerus head after image fusion. Image adopted from Reinhardt et al., 2006.

2.3 High-frequency Ultrasound (HFUS)

Ultrasound (US) uses a transducer to transmit sound pulses and to receive backscattered echo signals. Because the interfaces between tissues have different acoustic impedances and, therefore, different reflectivities, the received US signal contains boundary information of tissue with different elastic properties (T. Wang et al., 2011). US frequencies of 7.5-15 MHz are routinely used to visualize subcutaneous structures deeper than 1.5 cm including muscles, tendons, vessels and internal organs to identify pathologies or lesions (Aaslid et al., 2010; Shia et al., 2007; Tuzcu et al., 2010). The traditional US equipment used in the clinical environment

Determination of Melanoma Lateral and Depth Margins:
Potential for Treatment Planning and Five-Year Survival Rate
115

does not allow precise measurement of tissues due to insufficient spatial resolution (Ulrich et al., 1999). High-frequency ultrasound (HFUS), however, is capable of visualization of dermis (20 MHz) and even epidermis (50-100 MHz). The resolution of the image and depth of tissue penetration is largely dependent on the frequency of the US transducer. High-frequency scanners offer finer resolution (e.g., axial resolution of 50 µm and lateral resolution of 300 µm for a 20 MHz transducer) but poorer tissue penetration. HFUS at 20 MHz have been used with success to distinguish between benign skin lesions and CMM. Harland et al showed 100% sensitivity in distinguishing between 29 basal cell carcinomas and 25 CMMs (Harland et al., 2000). Bessoud et al in a study involving 111 patients, identified 65 of 70 CMMs (81%). There was a 100% sensitivity and specificity for melanoma and 32% specificity for non-melanoma lesions (Bessoud et al., 2003). HFUS at 20 MHz has also been shown to allow preoperative assessment of CMM thickness that correlated well with histological measurement (Dummer et al., 1995; Hoffmann et al., 1992; Lassau et al., 1999; Serrone et al., 2002; Tacke et al., 1995). A prospective study and systematic review of literature from 1987 to 2007 on CMM thickness measurement using 20 MHz HFUS reported that measurement of CMM thickness was possible except for thin CMMs (<0.4 mm) in areas with marked photoaging, and in the case of very thick CMMs exceeding the explored depth (7.6 mm) (Figure 5a) (Machet et al., 2009). This study also demonstrated a linear correlation between ultrasound and histology in CMM thickness measurements (Figure 5b). Another study using 75 MHz HFUS, involving 112 patients with suspicious CMMs, showed that 45 of 52 CMMs had clear hypoechogenic boundaries with tumor thicknesses ranging from 0 to 2.8 mm and correlation between HFUS measurement and histology was high (r=0.908) (Guitera et al., 2008).
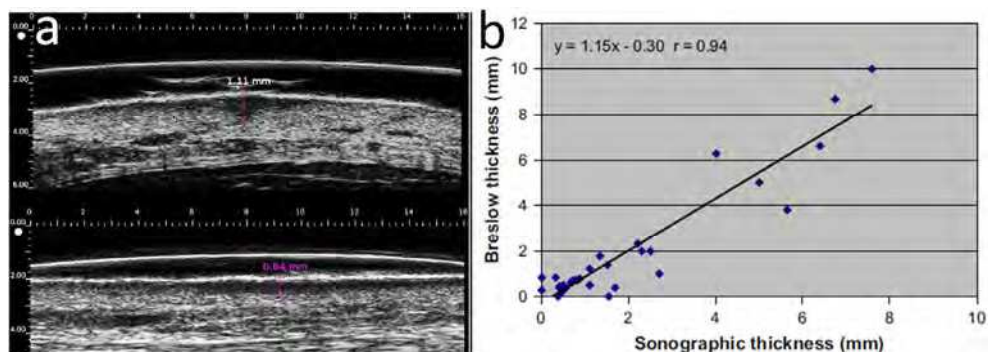

Fig. 5. (a) HFUS imaging of two CMM lesions. Lesions were generally hypoechoic and well demarcated from the dermis. (b) Linear relationship of CMM thickness between HFUS and histological measurements. Image adopted from Machet et al., 2009.

2.4 Optical Coherence Tomography (OCT)

OCT is an emerging diagnostic optical imaging technique that provides *in vivo* structure and function of tissues by measuring backscattered or backreflected light. OCT is based on the principle of Michelson interferometry. The light sources used for OCT imaging of skin are broad-band superluminescent diodes or tunable laser sources operating at a wavelength of about 1300 nm (Huang et al., 1991). The broad-band source leads to a small coherence length and achieves an axial and lateral resolution of approximately 15 µm and a penetration depth of

500 to 1000 µm (Olmedo et al., 2006; Welzel et al., 2003). OCT is a well established tool in ophthalmology (Welzel, 2003) and currently being advanced in dermatology (Fujimoto et al., 1995; Gambichler et al., 2005; Welzel, 2001), particularly for the diagnosis of CMM (Marghoob et al., 2003). A study of CMM characterization by OCT examined a panel of CMMs and benign nevi and demonstrated that CMMs showed increased architectural disarray, less defined dermal-epidermal borders, and vertically oriented icicle-shaped structures not seen in nevi (Figure 6b,c) (Gambichler et al., 2007). A recent review of OCT investigation in dermatology also showed that the intact border between epidermis and dermis disappears in infiltrative growing CMM compared with healthy skin (Figure 6a) (Smith & MacNeil, 2011).
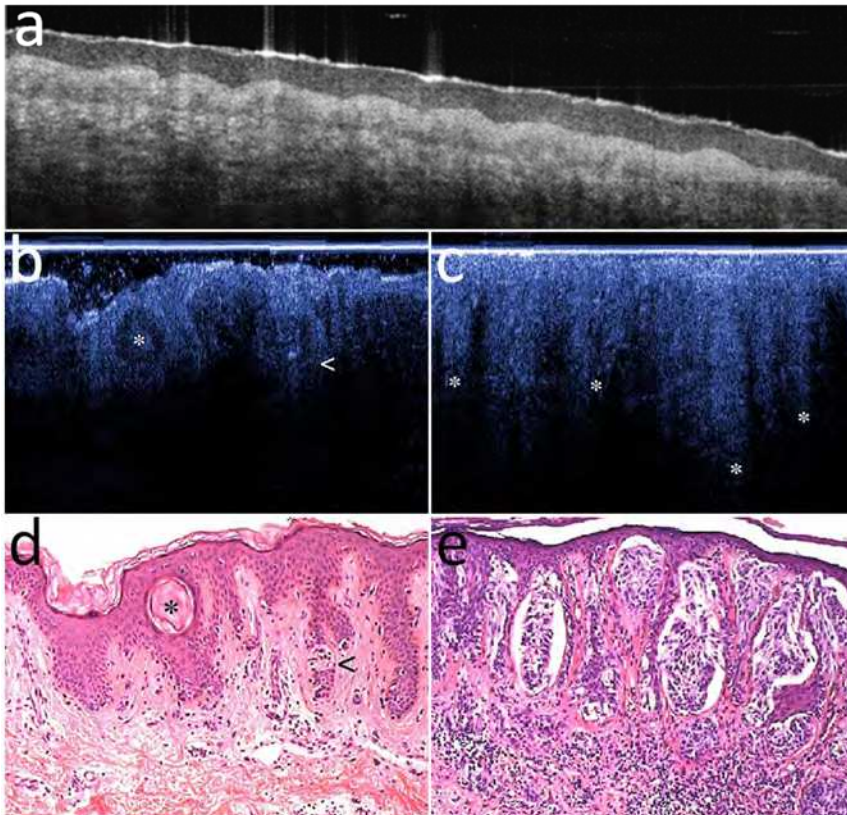

Fig. 6. (a) OCT image of health human finger tip skin. Image adopted from Smith & MacNeil, 2011. (b,d) OCT image of a compound nevi and corresponding histology, respectively. OCT displays finger-shaped elongated and broadened rete ridges including dense cell clusters (<) (b). Dermoepidermal junction zone is relatively clearly demarcated from more or less dark-appearing papillary dermis (b). Besides, epidermal horn cyst is demonstrated both on histology and OCT (*) (b and d). (c,e) OCT image of a superficial spreading CMM (0.91 mm) and corresponding histology, respectively. OCT (c) clearly displays marked architectural disarray including large vertically arranged icicle-shaped structures (*). Image adopted from Gambichler et al., 2007.

The utility of OCT for early-stage CMM thickness measurement (Figure 7) has not been fully established because correlation studies for CMM thickness determination by OCT and histology have not been reported. Furthermore, an important limitation of OCT is penetration depth. The maximum penetration depth of OCT is currently between 1-2 mm, dependent on the tissue type. Although the use of longer light wavelengths (e.g., 1750 nm) may improve penetration depth, no data is available to suggest that penetration depth greater than 4 mm is possible in the near future (Brezinski & Fujimoto, 1999). Therefore, OCT is currently not an established candidate for CMM thickness measurement.
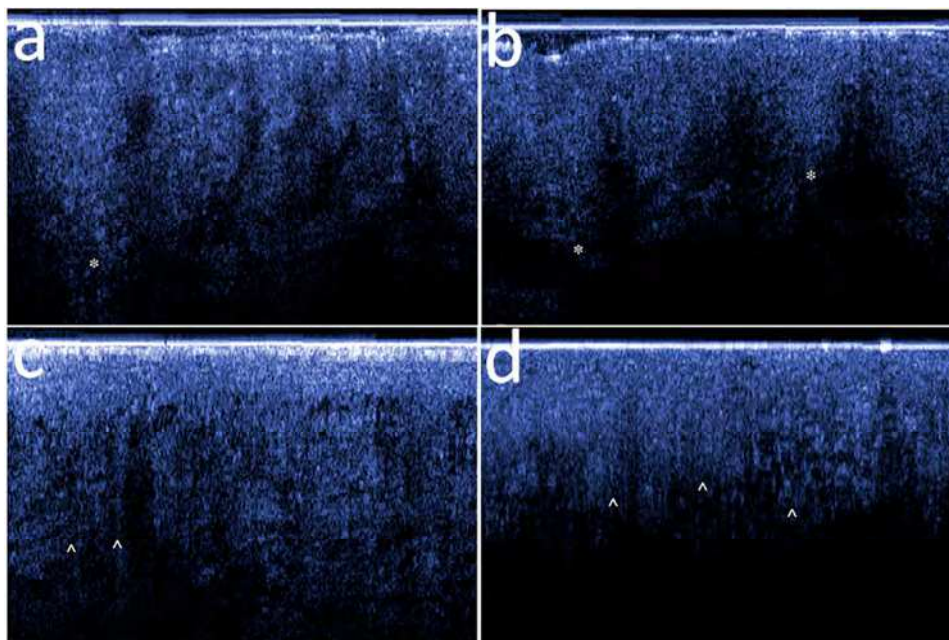

Fig. 7. OCT of 4 superficial spreading CMMs with Breslow thickness of (a) 0.45 mm, (b) 0.5 mm, (c) 0.7 mm, and (d) 1.6 mm measured by histology. CMM thickness determination is hardly possible. Despite large icicle-shaped structures (*) (a and b) and a patchy or cloudy bright dermis was observed (^) (c and d). Image adopted from Gambichler et al., 2007.

2.5 Photoacoustic Imaging (PAI)

PAI is an emerging hybrid technique that detects absorbed photons ultrasonically through the photoacoustic effect (Sun & Diebold, 1992). When a short-pulsed radiant source (e.g., laser) irradiates biological tissues, wideband ultrasonic waves (referred to as photoacoustic waves) are induced as a result of transient thermoelastic expansion. Magnitude of the photoacoustic waves is proportional to the local optical energy deposition and, hence, the waves divulge physiologically specific optical absorption contrast. As energy deposition is related to optical absorption coefficient of chromophores, concentration of multiple chromophores can be quantified by varying the laser excitation wavelength. Tissues such as blood vessels and CMM, can be imaged by PAI with the spatial resolution of ultrasound, which is not limited by the strong light scattering in biological tissues (X. Wang et al., 2003).

Images of microvasculature as deep as 3 mm were demonstrated with high-resolution PAI (Maslov et al., 2005). Recently, Oh et al used high-resolution and high-contrast PAI *in vivo* with a near-infrared (NIR) (764 nm) and a visible (584 nm) pulsed laser source, respectively, to image the 3-D CMM distribution inside nude mouse skin and the vascular system surrounding the CMM including tumor-feeding vessels (Oh et al., 2006). Maximum CMM thickness (0.5 mm) was measured with a lateral resolution of 45 μm and an axial resolution of 15 μm (Figure 8). Detection of melanoma cells in circulation was also reported (Holan & Viator, 2008; Weight et al., 2006; Zharov et al., 2006). More recently, in a pilot study Song et al proposed that non-invasive *in vivo* spectroscopic PAI can map sentinel lymph node using gold nanorods as lymph node tracers in a rodent model (Song et al., 2009).
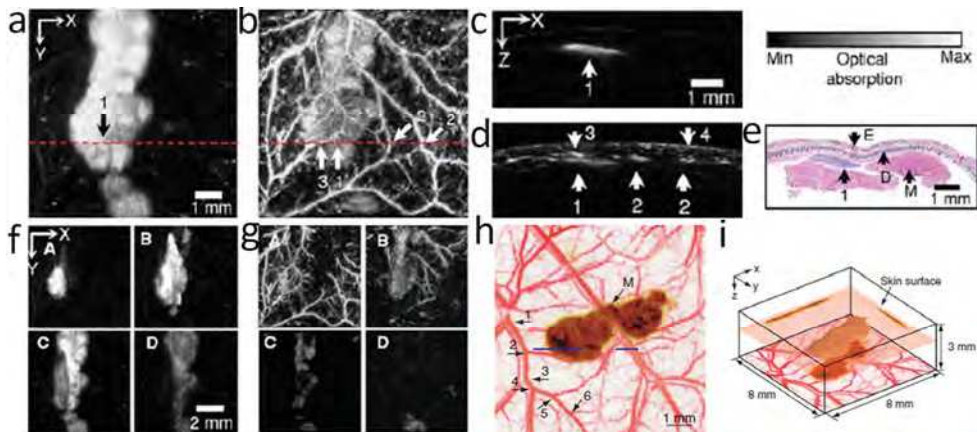

Fig. 8. *In vivo* non-invasive photoacoustic images of CMM and vascular distribution in nude mouse skin. (a,b) Enface photoacoustic images for the NIR light source (764 nm) and visible light source (584 nm), respectively: 1, CMM; 2, vessels perpendicular to image plane; 3, vessels horizontal to image plane; 4, skin. (c,d) Photoacoustic B-scan images from the NIR and visible light sources, respectively, for the dot lines in (a) and (b). (e) A cross-sectional histology image (H&E staining): E, epidermis; D, dermis; M, muscle. (f,g) Depthwise enface photoacoustic images from the NIR and visible light sources, respectively: A, 0.15-0.30 mm; B, 0.30-0.45 mm; C, 0.45-0.60 mm; D, 0.60-0.75 mm from the skin surface. Image adopted from Oh et al., 2006. (h) A composite of the two maximum amplitude projection (MAP) images projected along the z axis of a CMM region, where an MAP image is formed by projecting the maximum photoacoustic amplitudes along a direction to its orthogonal plane. Here, blood vessels are pseudocolored red in the 584 nm image and the CMM is pseudo-colored brown in the 764 nm image. As many as six orders of vessel branching can be observed in the image as indicated by numbers 1-6. (i) 3-D rendering of the CMM from the data acquired at 764 nm. Two MAP images at this wavelength projected along the x and y axes are shown on the two side walls, respectively. Image adopted from Zhang et al., 2006.

2.6 Pulsed Photothermal Radiometry (PPTR)

PPTR is a non-invasive technique that utilizes an infrared detector to measure radiometric temperature changes induced in a test material exposed to pulsed radiation. Heat generated as

a result of light absorption by subsurface chromophores in the test material diffuses to the surface and results in increased infrared emission levels. By collecting emitted radiation onto an infrared detector, a PPTR signal is obtained that represents the time evolution of temperature near the test-material surface. Useful information regarding the test material may be deduced from analysis of the PPTR signal. PPTR has been applied to depth profiling of strongly absorbing tissues and tissue phantoms (Milanič et al., 2007; Milner et al., 1996), including blood vessels in port wine stain (PWS) birthmarks in human skin (Li et al., 2004). Because different chromophore thicknesses can provide different laser induced initial temperature profiles and eventually produce different radiometric temperatures (T. Wang et al., 2009), the authors proposed that relationship between CMM thickness and detected radiometric temperature increase can be determined using PPTR in tissue phantoms mimicking CMM thicknesses from 120 μm to 2.8 mm (Figure 9) with a penetration depth of 1.7 mm and axial resolution of 75 μm (T. Wang et al., 2011). However, further studies are needed to investigate the capability of PPTR in CMM thickness measurement in skin *in vivo*.

2.7 Scanning Confocal Microscopy (SCM)

SCM is a non-invasive imaging technique that permits *in vivo* examination of the epidermis and papillary dermis. The basic premise of SCM is the selective collection of light from a specific plane in tissue through a pinhole-sized aperture which allows for light collection from the single in-focus plane and the rejection of light from all out-of-focus planes (Nehal et al., 2008). SCM has been recently employed in CMM diagnosis (Gerger et al., 2005; Marghoob & Halpern, 2005), preoperative and intraoperative margin assessment (Busam et al., 2001), and followup for response to medical treatment (Ahmed & Berth-Jones, 2000; Cornejo et al., 2000; Langley et al., 2006; Tannous et al., 2000, 2002). Commercial SCM instruments have been developed that image with lateral resolution of 0.5 to 1.0 μm and an optical sectioning thickness of 1.0 to 5.0 μm, to a depth of 200 to 300 μm in human skin (depth of papillary dermis). The spatial resolution of SCM is determined by the pinhole size while imaging depth is limited by the laser wavelength (with a 488 nm laser imaging 50-100 μm into skin (Gareau et al., 2007) and longer wavelengths lasers able to image at depths of up to 300 μm (Gonzalez & Gilaberte-Calzada, 2008; Marghoob et al., 2003; Nehal et al., 2008), providing images of the basement membrane down into the papillary dermis. SCM with an 830 nm light source is ideal for detecting CMM because melanin serves as an endogenous contrast agent. Melanin presence in melanocytic nevi and CMM provides strong contrast, thereby permitting the clear visualization of the architecture and outlines of cells (Gareau et al., 2008; Rajadhyaksha et al., 1995). SCM can be used in either fluorescence or reflectance modes (Meyer et al., 2006). While dermatological research tends to use fluorescence, clinical practice uses reflectance microscopy as this does not require fluorescent labeling of cells and tissues and, therefore, is more suitable for *in vivo* imaging. SCM criteria have been established to distinguish between CMMs and benign nevi (Gerger et al., 2005; Pellacani et al., 2007). Pellacani et al proposed a diagnostic algorithm that uses 2 major (i.e., nonedged dermal papillae and cytologic atypia at the basal layer) and 4 minor criteria (i.e., roundish pagetoid cells, widespread pagetoid infiltration in the epidermis, nucleated cells within dermal papillae, and cerebriform cell clusters in the dermis) (Figure 10) (Pellacani et al., 2005). The presence of at least 2 features, 1 major and 1 minor criterion, are required for a positive CMM diagnosis.
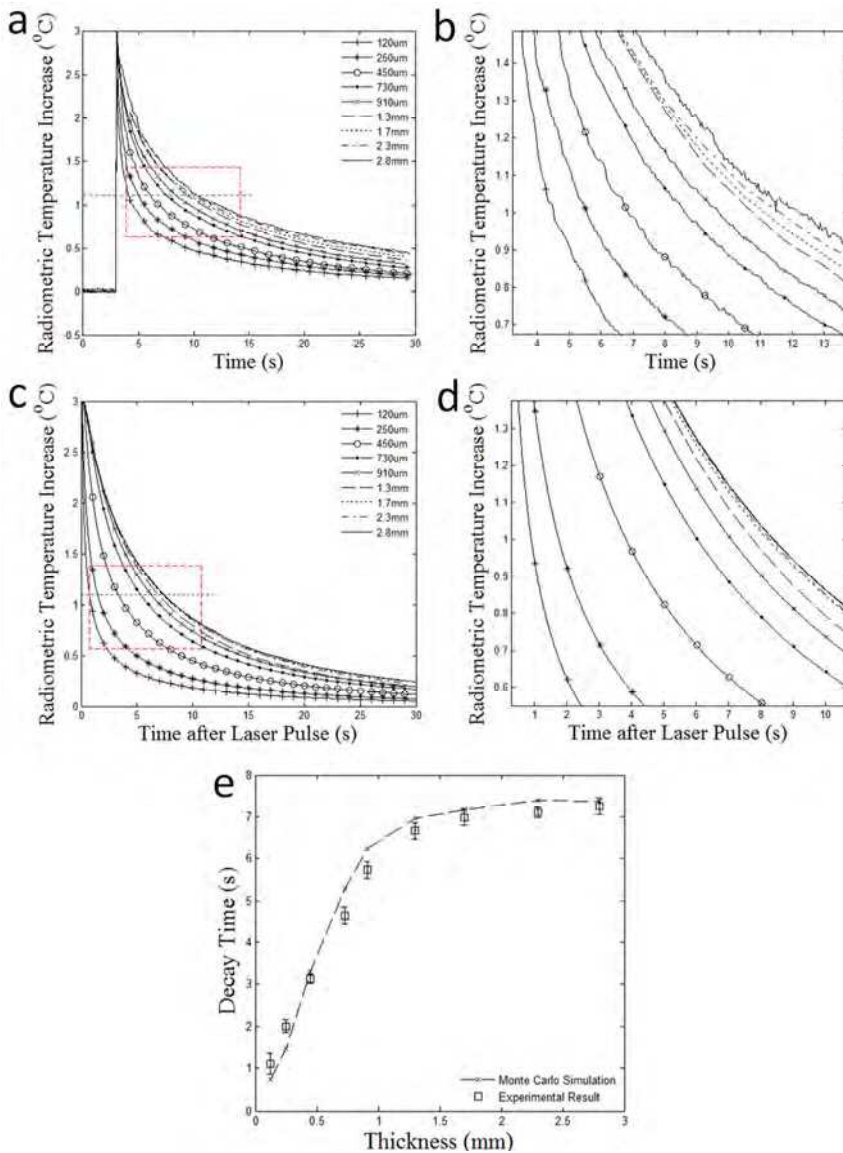
Fig. 9. (a) Measured radiometric temperature increase from PDMS tissue phantoms (top-layer is 120 μm-2.8 mm thick respectively - mimicking different CMM thicknesses). (b) Measured radiometric temperature increase in the window indicated in (a). (c) Simulated radiometric temperature increase. (d) Simulated radiometric temperature increase in the window indicated in (c). The dashed lines in (a,c) indicate when peak radiometric temperature increase decays to 37% of the maximum. (e) Decay time of the PDMS tissue phantoms with different top-layer thicknesses from experiment (square box) and simulation (dashed line). Image adopted from T. Wang et al., 2011.
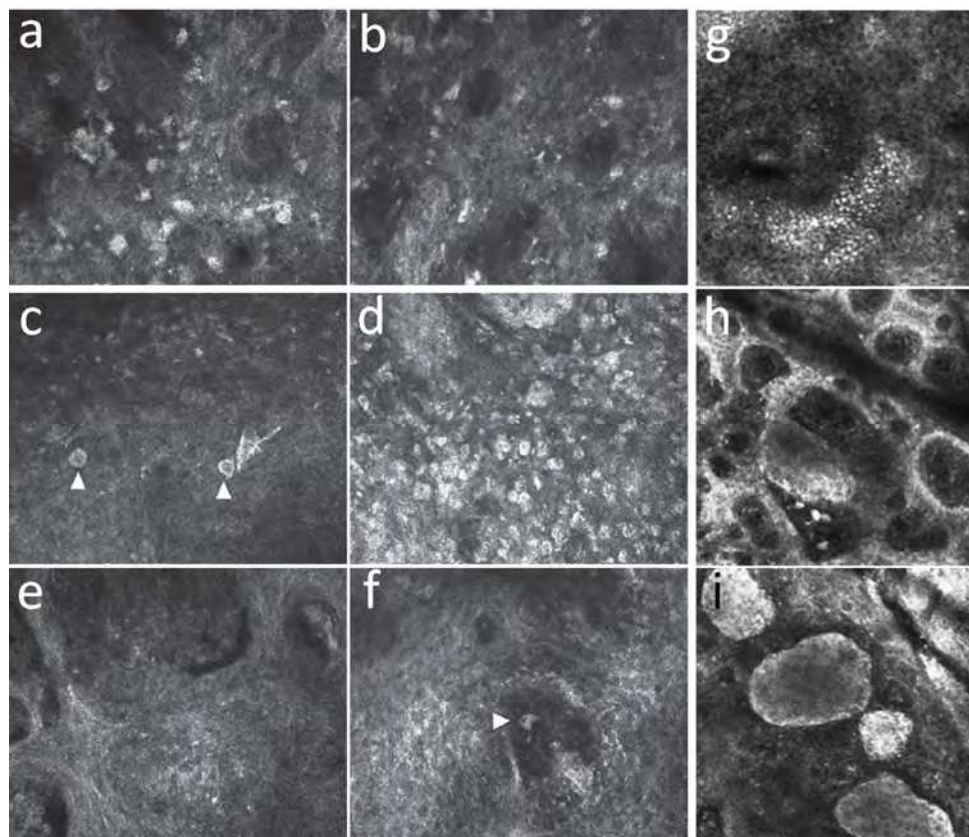
Fig. 10. *In vivo* reflectance-mode SCM images of characteristic CMM (corresponding to major (a,b) and minor (c,d,e,f) criteria) and benign nevi features (g,h,i): (a) Marked cytologic atypia at basal cell layers. (b) Nonedged papillae at dermoepidermal junction. (c) Roundish cells in superficial layers spreading upward in pagetoid fashion (arrowheads). (d) Pagetoid cells widespread throughout lesion. (e) Cerebriform clusters in papillary dermis. (f) Nucleated cells within dermal papilla (arrowhead). Image adopted from Pellacani et al., 2005. (g) Regular honeycombed and cobblestone pattern. (h) Regular junctional nests of cells (junctional cluster and junctional thickening); (i) Regular dense nests in the dermis. Image adopted from Pellacani et al., 2007.

SCM is capable to identify the lateral margins of CMM when determining the precise margins by clinical Wood's lamp or dermoscopic examination is virtually impossible. Chen et al reported a case of a patient with a recurrent CMM on the scalp that developed in a background of photodamage with diffuse melanocytic atypia and lentigines (Chen et al., 2005). SCM was able to distinguish the adjacent normal skin from CMM and the lateral tumor margin was preoperatively determined by SCM and the tumor was excised accordingly (Figure 11). Another study by Curiel-Lewandrowski also demonstrated the feasibility of using SCM in preoperative and intraoperative surgical margin assessment of indistinct CMM lesions (Curiel-Lewandrowski et al., 2004). However, SCM detection of

tumor depth margins is still difficult due to insufficient penetration depth. The high cost and sophisticated design of current SCM devices are considered to be major barriers. Efforts, such as miniaturizing the device and lowering the cost of production can facilitate wider adoption.
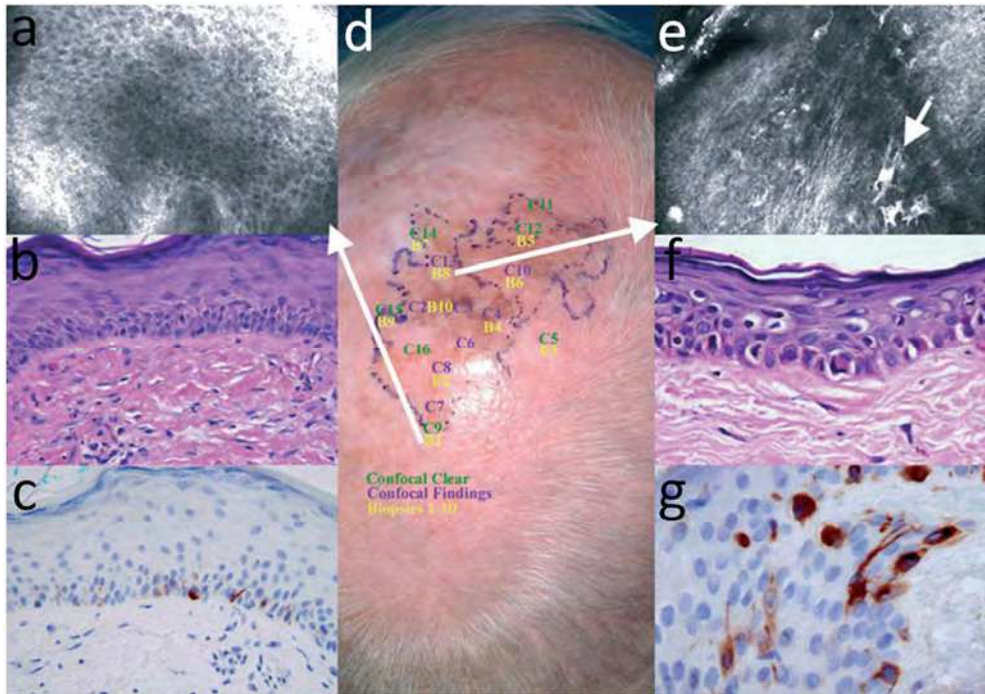

Fig. 11. (d) shows the refined border of the lentigo malignant melanoma (LMM) as determined by SCM. The SCM-examined foci are numbered 1-16 and are color-coded to indicate areas that were negative (green) and positive (purple) for LMM on SCM images. Five pairs (marked in yellow) of these foci on either side of the border were biopsied for histological confirmation. (a), (b) and (c) are the confocal, histology and Melan-A immunostained sections of one representative area of normal skin (long arrow in (d)). (a) shows the epidermal layer and demonstrates the honeycomb pattern of keratinocytes and well-defined cell to cell demarcations which is the characteristic architecture of normal skin. (b,c) The haematoxylin and eosin (H&E)-stained and Melan-A-stained histological sections of normal skin, respectively. (e,f,g) Confocal, histology and Melan-A immunostained sections of one representative area of skin with LMM (long arrow in (d)). (e) shows the spinous layer and demonstrates pagetoid spread of atypical, dendritic melanocytes (short arrow), loss of the normal architecture and a grainy background-all features consistent with LMM. (f,g) H&E-stained and Melan-A-stained histological sections of LMM, respectively. The Melan-A staining (g) shows the dendrites of the melanoma cell and correlates with the dendritic malignant melanocyte (arrow) seen in (e). Image adopted from Chen et al., 2005.

2.8 Multi-photon Luminescence Microscopy (MPLM) and Second Harmonic Generation (SHG)

MPLM is a rapidly developing imaging technique in the field of optical sectioning, which has been applied to tissue imaging with intrinsic fluorescence (Zipfel et al., 2003a, 2003b). Endogenous fluorophores such as melanin, elastin and collagen are sources of tissue fluorescence. MPLM of animal and human skin has been reported by So et al, Masters et al, Hendriks et al, König et al and Peuckert et al (Hendriks & Lucassen, 1999; König, 2000a, 2000b, 2002; Masters et al., 1998; Peuckert et al., 2000; So & Kim, 1998). Teuchner et al reported MPLM detection of melanin fluorescence (Teuchner et al., 1999). MPLM excites fluorophores by a non-linear multiphoton (e.g., two-photon) process, as opposed to the single photon excitation used in conventional microscopy. Two-photon excitation occurs when two photons of approximately half the one photon energy are absorbed nearly simultaneously by the fluorescent molecule. MPLM allows non-invasive tissue screening with subcellular spatial resolution. Wang et al demonstrated that lateral and axial resolution of MPLM can reach about 0.3 and 1 µm, respectively (H. Wang et al., 2005). Masters et al detected the autofluorescence of human skin in depths down to 200 µm (Masters et al., 1997). Figure 12 illustrates the effectiveness of MPLM in obtaining subcellular resolution images of CMM and normal skin (Dimitrow et al., 2009).
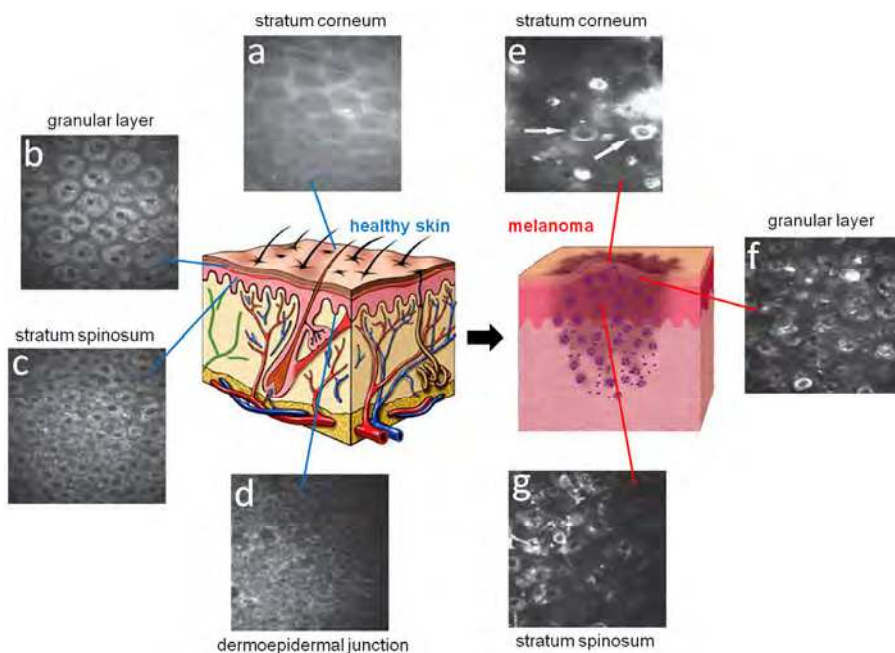

Fig. 12. MPLM of healthy human skin (a,b,c,d) and melanoma (e,f,g) with subcellular resolution. Optical sections of healthy skin were captured at the same skin site, but at different tissue depths showing: (a) the stratum corneum, (b) the granular layer, (c) the stratum spinosum and (d) the dermoepidermal junction; Optical sections of melanoma: (e) The stratum corneum characterized by highly fluorescent melanocytes marked by white arrows. (f) The granular layer characterized by large intercellular distance. (g) The spinous layer characterized by poorly defined keratinocyte cell borders. Image modified from Dimitrow et al., 2009.

Similar to SCM, MPLM has the potential to precisely measure the lateral margins of CMM, however, limited penetration depth prevents use for tumor depth margin delineation.

SHG (also called frequency doubling) is also a nonlinear optical process, in which photons interacting with a nonlinear material are effectively combined to form new photons with twice the energy and, therefore, twice the frequency and half the wavelength of the incident photons (Fine & Hansen, 1971; Roth & Freund, 1979; Theodossiou et al., 2006). Because SHG excitation wavelength is off the resonance wavelength of chromophores in tissue, less energy is absorbed, and hence, negligible thermal or photodamage is observed (Lohela & Werb, 2010). Recently, SHG imaging has been employed to detect noncentrosymmetric crystalline structures (e.g., collagen) in tissues (Campagnola et al., 2001; Cox et al., 2003; Lim et al., 2010; H. Wang et al., 2009). Thrasivoulou et al demonstrated that SHG imaging showed detailed collagen distribution in healthy skin, with total absence of SHG signal (fibrillar collagen) within the melanoma-invaded tissue (Figure 13) (Thrasivoulou et al., 2011). The presence or absence of SHG signal changed dramatically at the borders of CMM, allowing accurate demarcation of CMM margins that strongly correlated with H&E and Melan-A defined margins ($p<0.002$).
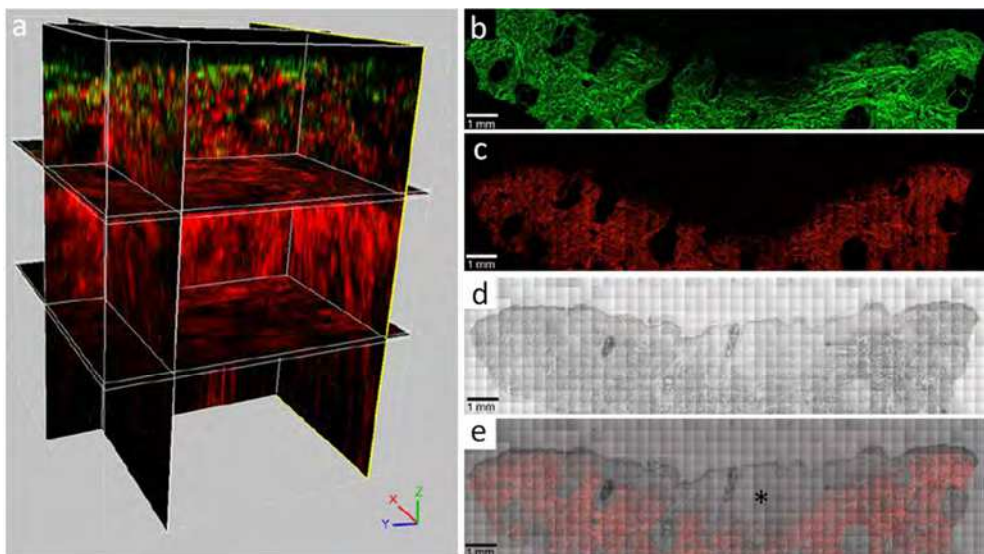

Fig. 13. (a) SHG imaging of healthy, *ex vivo*, human skin sample showing collagen morphology throughout the entire thickness when imaged from the epidermis, in the transmission (red) and backscattered (green) geometry. The whole thickness of epidermis and dermis to depths of approximately 300 µm in the backscattered geometry and over 1000 µm in the transmission geometry were imaged, respectively. Montage of SHG images of CMM in (b) transmission, (c) backscattered geometry, and (d) bright-field image. (e) Superimposed image of bright-field and SHG images indicates collagen distribution within each section. (*) indicates the CMM location in (e). Image modified from Thrasivoulou et al., 2011.

Determination of Melanoma Lateral and Depth Margins:
Potential for Treatment Planning and Five-Year Survival Rate
125

2.9 Dermoscopy

Dermoscopy (also called dermatoscopy, skin surface microscopy, epiluminescence microscopy) is a non-invasive technique for the early recognition of CMM. Dermoscopy was first introduced to evaluate pigmented lesions in 1971 (MacKie, 1971), studied rigorously in Europe and Australia during the 1980s and 1990s (Argenziano et al., 1998), and adopted slowly in the United States in recent years (Tripp et al., 2002). To date, dermoscopic and histologic correlations and algorithms for dermoscopic diagnosis of CMM have been established (Argenziano et al., 2003; Henning et al., 2007). Two types of dermoscopes are currently available: (1) nonpolarized dermoscope (NPD) and (2) polarized dermoscope (PD). NPD uses liquid (e.g., oil, water, or alcohol gel) to cover the lesion, which decreases light reflection, refraction, and diffraction, makes the epidermis essentially translucent and allows for visualization of subsurface anatomic structures of the epidermis and papillary dermis (Figure 14). PD uses a polarizer that preferentially captures backscattered light from below the surface of the skin. The liquid or direct contact with the skin is not needed. However, some subset of CMMs (e.g., amelanotic/hypomelanotic CMMs that lack pigmentations and dermoscopic structures) are difficult to diagnose with dermoscopy and, thus, impossible to determine lateral margins by dermoscopy. Although a dermoscopic image can show subsurface structures of CMM, this approach is a 2-D imaging technique that cannot obtain a depth profile of the lesion. Therefore, depth margins of melanoma are not provided by dermoscopy.
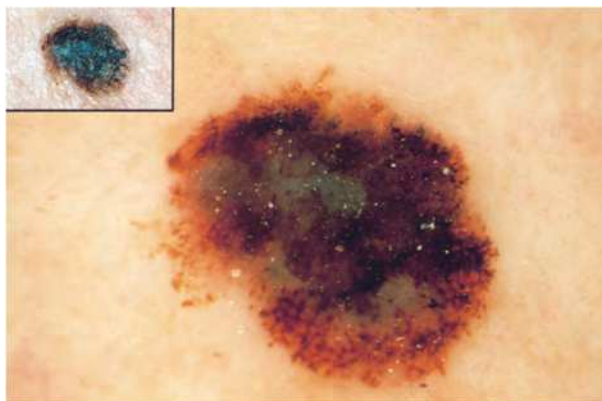

Fig. 14. Superficial spreading CMM viewed with dermoscopy (large panel) and with the unaided eye (inset panel). Compared with the unaided eye, dermoscopy reveals several additional structural features, which are typical of CMM, including irregular dots and irregular extensions (pseudopods) in the periphery and a blue-whitish veil. Image adopted from Kittler et al., 2002.

2.10 Multispectral Imaging (MSI), Diffuse Reflectance Spectroscopy (DRS) and Raman Spectroscopy (RS)

MSI has been widely used in the fields of astronomy and remote sensing (Colarusso et al., 1998; Curran, 1994) and, recently, is being applied to the field of biology and medicine (Johnson et al., 2007; Mansfield et al., 2005; Weber et al., 2011). An essential part of an MSI

microscope is a spectral dispersion element that separates incident light into its spectral components (i.e., 400-1000 nm) (Bearman & Levenson, 2003). MSI of skin acquires spectrally resolved information at each pixel of a multispectral image, providing information on the distributions of collagen, melanin content and blood vessels within skin lesions (Marchesini, 1991, 1992). Carrara et al developed an algorithm for the automatic segmentation of multispectral images of 1856 cutaneous pigmented lesions including 264 CMMs, which successfully detected lateral margins of the lesions with a contour accuracy of 97.1% (Carrara et al., 2005). Marchesini et al reported that MSI and an artificial neural network could be used in the preoperative evaluation of CMM thickness with sensitivity (i.e., CMM≥0.75 mm thick correctly classified) and specificity (i.e., CMM<0.75 mm thick correctly classified) ranging from 76 to 90% and from 91 to 74%, respectively (Marchesini et al., 2007).

DRS (also called elastic scattering spectroscopy) measures the spectral modification of remitted light (i.e., light that has propagated some distance into the skin, been scattered, and recollected at skin surface). DRS was first introduced as a single-point measurement technique by Marchesini et al in 1992 to study CMM and nevus with a 5 mm probe (Marchesini et al., 1992). Wallace et al later reported that DRS in the wavelength range 320-1100 nm had the potential for improving the differential diagnosis of CMM from benign pigmented skin lesions (Wallace, 2000a, 2000b). However, further prospective study of DRS is needed to investigate its capability to detect tumor margins.

RS is a non-invasive imaging technique that has been widely used for the past 70 years for nondestructive chemical analysis. RS is based on the principle of Raman scattering, the inelastic scattering of electromagnetic radiation. The Raman scattering effect is caused by molecular vibrations in the irradiated sample and thus gives information about the structure of the molecules. Earlier studies have shown that samples of various benign skin lesions and nonmelanoma skin cancer have characteristic Raman spectra (Gniadecka et al., 1997a, 1997b, 1998). Recent studies on basal cell carcinoma by RS demonstrated its feasibility to distinguish malignant tissue from healthy surrounding tissue (Nijssen et al., 2002). More recently, Gniadecka et al developed a neural network system for the automated classification of Raman spectra, allowing CMM differentiation from other clinically similar skin tumors (Gniadecka et al., 2004). Therefore, RS is potentially capable of demarcating lateral margins of CMM.

In contrast to other imaging techniques (e.g., dermoscopy), MSI, DRS and RS are more objective and not observer dependent. However, similar to demoscopy, MSI, DRS and RS are also 2-D imaging techniques that cannot image the depth profile of CMM directly. Therefore, detection of depth margins of CMM by MSI, DRS or RS is hardly possible.

3. Conclusion

Early detection and surgical resection can reduce CMM mortality. To this end, several non-invasive imaging techniques have been developed to realize CMM screening, early diagnosis, preoperative tumor staging, surgical margin definition and *in vivo* tumor monitoring over multiple time points. Currently available instruments include MRI, CT, PET, HFUS, OCT, PAI, PPTR, SCM, MPLM, SHG, dermoscopy, MSI, DRS and RS. Dermoscopy, MSI, DRS and RS are useful in the evaluation of superficial CMMs, but they are not depth resolved. PET/CT do not have the resolution to detect early stage CMMs (e.g., <1 mm). They can, however, be used to detect tumor metastasis. MRI has comparable or higher resolution than CT and, hence, is suited to imaging advanced tumor invasion (e.g., >1 mm). SCM, MPLM and SHG provide physicians with an unprecedented capability

to visualize a CMM lesion at a detail comparable to histology, but their imaging depths are limited to several hundred micrometers from skin surface, preventing them from detection of CMM depth margins beyond penetration depth. HFUS, OCT, PAI and PPTR have spatial resolutions and penetration depths between MRI/CT/PET and SCM/MPLM/SHG, therefore, they are potentially capable of detecting both lateral and depth margins of CMMs. A comparison of spatial resolution, penetration depth, sensitivity/specificity, correlation with histology and temporal monitoring (possibility to monitor CMM changes at multiple time points) of the imaging techniques discussed are summarized in Table 2 below.

From a clinical perspective, sensitivity and specificity studies of CMM diagnosis by MRI/CT/PET, HFUS, SCM/MPLM and dermoscopy/MSI/DRS/RS having been performed. Although sensitivity and specificity of OCT, PAI, PPTR and SHG on human CMM diagnosis are not yet established, they are promising imaging techniques that need further investigation on not only CMM diagnosis but also tumor lateral and depth margin delineation. To date, surgical resection is the major treatment for primary CMMs, which significantly increases the five-year survival rate. Surgical margins are currently determined by CMM thickness measured from biopsy with histology – the gold standard. The imaging techniques discussed, however, have the potential to non-invasively measure CMM thickness and detect tumor margins, and even guide CMM surgical resection in real time, which will reduce unnecessary biopsies and, eventually replace this invasive approach.

Because each of these imaging techniques has advantages and shortcomings, the best performing imaging tool for CMM evaluation is a combination of different imaging techniques – although at increased cost. A multimodal imaging tool will significantly improve the accuracy of CMM identification as well as the precision of surgical margin definition, which would achieve the five-year survival rate currently determined by biopsy-based surgical resection.

Imaging Techniques	Spatial Resolution (Lateral/Axial)	Penetration Depth	Sensitivity/Specificity in CMM Diagnosis	Correlation (R) with Histology	Temporal Monitoring
MRI	0.04-0.5 mm/ 0.3-0.5 mm†	Whole body	79.8%/76.4%[1]	NA	Yes
CT	0.1-0.29 mm/ 0.1-1 mm$	Whole body	77.1%/69.9%[1]	NA	Yes
PET	1-4 mm/ 1-4 mm*	Whole body	70.4%/83.7%[1]	NA	Yes
HFUS	20-300 µm/ 20-50 µm§	4-7.6 mm§	100%/32%[2]	>0.96[2]	Yes
OCT	10 µm/ 10-20 µm¶	1-2 mm	NA	NA	Yes
PAI	45 µm/15 µm	3 mm	NA	NA	Possible
PPTR	50 µm/75 µm	1.7 mm	NA	NA	Possible
SCM	0.5-1 µm/ 1-5 µm	200-300 µm	91%/99%[3]	NA	Possible
MPLM	0.3 µm/1 µm	200 µm	84%/76%[4]	NA	Possible

Imaging Techniques	Spatial Resolution (Lateral/Axial)	Penetration Depth	Sensitivity/Specificity in CMM Diagnosis	Correlation (R) with Histology	Temporal Monitoring
SHG	0.5 µm/ 1-1.9 µm[δ]	550 µm[ζ]	NA	0.9924[5]	Possible
Dermoscopy	20 µm/NA[ζ]	NA	96.3%/70.4%[6]	NA	Yes
MSI	30 µm/NA[η]	NA	76-90%/91-74%[7]	0.33[7]	Possible
DRS	200 µm/NA[κ]	NA	100%/84.4%[8]	NA	Possible
RS	100 µm/NA[µ]	NA	85%/99%[9]	NA	Possible

[†] Lateral resolution varies from 0.04 (9.4 T) to 0.7 mm (3 T), axial resolution varies from 0.3 (9.4 T) to 0.5 mm (3 T) (Gammal et al., 1996; Schick, 2005).

[$] Lateral resolution varies from 0.1 (micro-CT) to 0.29 mm (conventional CT), axial resolution varies from 0.1 (micro-CT) to 1 mm (conventional CT) (Badea et al., 2004; Schroeder et al., 2001).

[*] Both lateral and axial resolution vary from nearly 1 mm FWHM (2 mm FWTM) for a 10-20 cm diameter system typical for animal studies with ^{18}F to roughly 4 mm FWHM (7 mm FWTM) for an 80 cm diameter system typical for human imaging using ^{15}O (Levin & Hoffman, 1999).

[§] Lateral resolution varies from 20 (100 MHz) to 300 µm (20 MHz), axial resolution varies from 20 (100 MHz) to 50 µm (20 MHz), penetration depth varies from 4 (100 MHz) to 7.6 mm (20 MHz) (Harland et al., 1993; Passmann & Ermert, 1999; Pavlin et al., 1990).

[¶] Lateral resolution can be 10 µm or better, axial resolution varies from 10 to 20 µm (Ding et al., 2002; Schenk & Brezinski, 2002).

[δ] Axial resolution varies from 1 to 1.9 µm (Campagnola et al., 2002; Moreaux et al., 2000).

[ζ] Lateral resolution is 20 µm with no axial resolution (Kopf et al., 1997).

[η] Lateral resolution is 30 µm with no axial resolution (Marchesini et al., 2007).

[κ] Lateral resolution is limited by the fiber size, no axial resolution is available (Häggblad et al., 2010).

[µ] Lateral resolution is limited by the laser spot size, no axial resolution is available (Gniadecka et al., 2004).

[1] 420 stage III/IV melanoma lesions from 64 patients were examined by MRI, CT and PET respectively (Pfannenberg et al., 2007).

[2] 114 pigmented skin lesions including 65 CMMs were examined by 20 MHz HFUS, ultrasound and histological measurement of melanoma thickness strongly correlated (Bessoud et al., 2003).

[3] 162 skin lesions including 27 CMMs were examined by SCM (Gerger et al., 2006).

[4] 100 melanocytic skin lesions including 26 CMMs from 83 patients were examined by MPLM (Dimitrow et al., 2009).

[5] Correlation of collagen fiber density was examined from mid-point of CMM lesion to deep area of non-lesion skin (Thrasivoulou et al., 2011).

[6] 128 pigmented skin lesions including 33 CMMs were examined by dermoscopy and ABCD diagnosis rule (Argenziano et al., 2003).

[7] 1939 pigmented skin lesions including 250 CMMs were examined by MSI, the correlation coefficient value between tumor thickness and area is not so great to fully assess that lesion dimension increases with thickness (Marchesini et al., 2007).

[8] 15 CMMs and 32 compound naevi were examined by DRS (Wallace, 2000a).

[9] 134 pigmented skin lesions including 22 CMMs were examined by RS and neural network analysis (Gniadecka et al., 2004).

Table 2. Comparison of non-invasive imaging techniques for CMM diagnosis and tumor margin detection in terms of spatial resolution, penetration depth, sensitivity/specificity, correlation with histology and temporal monitoring (possibility to monitor CMM changes at multiple time points)

4. Acknowledgement

5. References

Aaslid, R.; Huber, P. & Nornes, H. (1984). Evaluation of Cerebrovascular Spasm with Transcranial Doppler Ultrasound. *Journal of Neurosurgery*, Vol.60, No.1, (January 1984), pp. 37-41

Ahmed, I. & Berth-Jones, J. (2000). Imiquimod: a Novel Treatment for Lentigo Maligna. *British Journal of Dermatology*, Vol.143, No.4, (October 2000), pp. 843–845

Akcali, C.; Zincirkeser, S.; Erbagcy, Z.; Akcali, A.; Halac, M.; Durak, G.; Sager, S. & Sahin, E. (2007). Detection of Metastases in Patients with Cutaneous Melanoma Using FDG-PET/CT. *Journal of International Medical Research*, Vol.35, No.4, (July 2007), pp. 547-553

American Cancer Society, (Last medical review: March 5, 2010), 06.01.2011, Available from http://www.cancer.org/Cancer/SkinCancerMelanoma/DetailedGuide/melanoma-skin-cancer-key-statistics

Argenziano, G.; Fabbrocini, G.; Carli, P.; Giorgi, V. D.; Sammarco, E. & Delfino, M. (1998). Epiluminescence Microscopy for the Diagnosis of Doubtful Melanocytic Skin Lesions. Comparison of the ABCD Rule of Dermatoscopy and a New 7-Point Checklist Based on Pattern Analysis. *Archives of Dermatology*, Vol.134, (December 1998), pp. 1563-1570

Argenziano, G.; Soyer, H. P.; Chimenti, S.; Talamini, R.; Corona, R.; Sera, F.; Binder, M.; Cerroni, L.; Rosa, G. D. & Ferrara, G. (2003). Dermoscopy of Pigmented Skin Lesions: Results of a Consensus Meeting via the Internet. *Journal of the American Academy of Dermatology*, Vol.48, No.5, (May 2003), pp. 679-693

Armstrong, P. & Wastie, M. L. (Eds.). (2001). *A Concise Textbook of Radiology*, Arnold, pp. 536-594, ISBN 0340759380-9780340759387, London, UK

Baddeley, H. (1984). *Radiological Investigation. A Guide to the Use of Medical Imaging in Clinical Practice*, Wiley Medical Publications, Ann Arbor, MI, USA

Badea, C.; Hedlund, L. W. & Johnson, G. A. (2004). Micro-CT with Respiratory and Cardiac Gating. *Medical Physics*, Vol.31, No.12, (November 2004), pp. 3324-3329

Balch, C. M. & Ross, M. I. (1999). Sentinel Lymphadenectomy for Melanoma-Is It a Substitute for Elective Lymphadenectomy?. *Annals of Surgical Oncology*, Vol.6, No.5, (May 1999), pp. 416-417

Balch, C. M.; Buzaid, A.C.; Soong, S.J.; Atkins, M. B.; Cascinelli, N.; Coit, D. G.; Fleming, I. D.; Gershenwald, J. E.; Houghton, A.; Kirkwood, Jr J. M.; McMasters, K. M.; Mihm, M. F.; Morton, D. L.; Reintgen, D. S.; Ross, M. I.; Sober, A.; Thompson, J. A. & Thompson, J. F. (2001). Final Version of the American Joint Committee on Cancer (AJCC) Staging System for Cutaneous Melanoma. *Journal of Clinical Oncology*, Vol.19, No.16, (August 2001), pp. 3635–3648

Bearman, G. & Levenson, R. (2003). Biological Imaging Spectroscopy, In: *Biomedical Photonics Handbook*, Vo-Dinh, T. (Ed.), CRC Press, pp. 8.1–8.26, ISBN 0849311160, Boca Raton, FL, USA

Belhocine, T. Z.; Scott, A. M.; Even-Sapir, E.; Urbain, J. L. & Essner, R. (2006). Role of Nuclear Medicine in the Management of Cutaneous Malignant Melanoma. *Journal of Nuclear Medicine*, Vol.47, No.6, (June 2006), pp. 957–967

Bessoud, B.; Lassau, N.; Koscielny, S.; Longvert, C.; Avril, M.; Duvillard, P.; Rouffiac, V.; Leclère, J. & Roche, A. (2003). High-frequency Sonography and Color Doppler in the Management of Pigmented Skin Lesions. *Ultrasound in Medicine and Biology*, Vol.29, No.6, (June 2003), pp. 875-879

Bittoun, J.; Saint-Jalmes, H.; Querleux, B. G.; Darrasse, L.; Jolivet, O.; Idy-Peretti, I.; Wartski, M.; Richard, S. B. & Leveque, J. L. (1990). In Vivo High-Resolution MR Imaging of the Skin in a Whole-Body System at 1,5 T. *Radiology*, Vol.176, (August 1990), pp. 457–460

Blessing, C.; Feine, U.; Geiger, L.; Carl, M.; Rassner, G. & Fierlbeck, G. (1995). Positron Emission Tomography and Ultrasonography: a Comparative Retrospective Study Assessing the Diagnostic Validity in Lymph Node Metastases of Malignant Melanoma. *Archives of Dermatology*, Vol.131, No.12, (1995), pp. 1394-1398, ISSN 0003-987X

Boni, R.; Böni, R.; Steinert, H.; Burg, G.; Buck, A.; Marincek, B.; Berthold, T.; Dummer, R.; Voellmy, D.; Ballmer, B. & Von Schulthess, G. (1995). Staging of Metastatic Melanoma by Whole-Body Positron Emission Tomography Using 2-fluorine-18-fluoro-2-deoxy-D-glucose. *British Journal of Dermatology*, Vol.132, No.4, (April 1995), pp. 556–562

Breslow, A. (1970). Thickness, Cross Sectional Areas and Depth of Invasion in the Prognosis of Cutaneous Melanoma. *Annals of Surgery*, Vol.172, (November 1970), pp. 902-908

Brezinski, M. E. & Fujimoto, J. G. (1999). Optical Coherence Tomography: High-Resolution Imaging in Nontransparent Tissue, *IEEE Journal of Selected Topics in Quantum Electronics*, Vol.5, No.4, (July-August 1999), pp. 1185-1192

Busam, K. J.; Hester, K.; Charles, C.; Sachs, D. L.; Antonescu, C. R.; Gonzalez, S. & Halpern, A. C. (2001). Detection of Clinically Amelanotic Malignant Melanoma and Assessment of Its Margins by In Vivo Confocal Scanning Laser Microscopy. *Archives of Dermatology*, Vol.137, (July 2001), pp. 923-929

Campagnola, P. J.; Clark,H. A.; Mohler, W. A.; Lewis, A. & Loew, L. M. (2001). Second-Harmonic Imaging Microscopy of Living Cells. *Journal of Biomedical Optics*, Vol.6, No.3, (July 2001), pp. 277–286

Campagnola, P. J.; Millard, A. C.; Terasaki, M.; Hoppe, P. E.; Malone, C.J. & Mohler, W.A. (2002). Three-Dimensional High-Resolution Second-Harmonic Generation Imaging of Endogenous Structural Proteins in Biological Tissues. *Biophysical Journal*, Vol.82, No.1, (January 2002), pp. 493-508

Cancer Facts and Figures 2010. (2010). *American Cancer Society*, 06.06.2011, Available from http://www.cancer.org/acs/groups/content/@epidemiologysurveilance/documents/document/acspc026238.pdf

Carrara, M.; Tomatis, S.; Bono, A.; Bartoli, C.; Moglia, D.; Lualdi, M.; Colombo, A.; Santinami M. & Marchesini, R. (2005). Automated Segmentation of Pigmented Skin Lesions in Multispectral Imaging. *Physics in Medicine and Biology*, Vol.50, No.22, (November 2005), pp. N345-N357

Chen, C. S.; Elias, M.; Busam, K.; Rajadhyaksha, M. & Marghoob, A. (2005). Multimodal In Vivo Optical Imaging, Including Confocal Microscopy, Facilitates Presurgical Margin Mapping for Clinically Complex Lentigo Maligna Melanoma. *British Journal of Dermatology*, Vol.153, No.5, (November 2005), pp. 1031–1036

Colarusso, P.; Kidder L. H.; Levin, I. W.; Fraser, J. C.; Arens, J. F. & Lewis, E. N. (1998). Infrared Spectroscopic Imaging: from Planetary to Cellular Systems. *Applied Spectroscopy*, Vol.52, No.3, (March 1998), pp. 106A-120A

Cornejo, P.; Vanaclocha, F.; Polimon, I. & Del Rio, R. (2000). Intralesional Interferon Treatment of Lentigo Maligna. *Archives of Dermatology*, Vol.136, No.3, (March 2000), pp. 428-430

Cox, G.; Kable, E.; Jones, A.; Fraser, I.; Manconi, F. & Gorrell, M. D. (2003). 3-dimensional Imaging of Collagen Using Second Harmonic Generation. *Journal of Structural Biology*, Vol.141, No.1, (January 2003), pp. 53-62

Curiel-Lewandrowski, C.; Williams, C. M.; Swindells, K. J.; Tahan, S. R.; Astner, S.; Frankenthaler, R. A. & Gonzalez, S. (2004). Use of In Vivo Confocal Microscopy in Malignant Melanoma: an Aid in Diagnosis and Assessment of Surgical and Nonsurgical Therapeutic Approaches. *Archives of Dermatology*, Vol.140, No.9, (2004), pp. 1127-1132, ISSN 0003-987X

Curran, P. J. (1994). Imaging Spectrometry. *Progress in Physical Geography*, Vol.18, No.2, (June 1994), pp. 247-266

Damian, D. L.; Fulham, M. J.; Thompson, E. & Thompson, J. F. (1996). Positron Emission Tomography in the Detection and Management of Metastatic Melanoma. *Melanoma Research*, Vol.6, No.4, (August 1996), pp. 325-329

Dimitrow, E.; Ziemer, M.; Koehler, M. J.; Norgauer, J.; König, K.; Elsner, P. & Kaatz, M. (2009). Sensitivity and Specificity of Multiphoton Laser Tomography for In Vivo and Ex Vivo Diagnosis of Malignant Melanoma. *Journal of Investigative Dermatology*, Vol.129, (January 2009), pp. 1752-1758

Ding, Z; Ren, H; Zhao, Y.; Nelson, J. S. & Chen, Z. (2002). High-resolution Optical Coherence Tomography over a Large Depth Range with an Axicon Lens. *Optics Letters*, Vol.27, No.4, (February 2002), pp. 243-245

Dummer, W.; Blaheta, H. J.; Bastian, B. C.; Schenk, T.; Brocker, E. V. & Remy, W. (1995). Preoperative Characterization of Pigmented Skin Lesions by Epiluminescence Microscopy and High-frequency Ultrasound. *Archives of Dermatology*, Vol.131, No.3, (1995), pp. 279–285

Edge, S. B.; Byrd, D. R.; Compton, C. C.; Fritz, A. G.; Greene, F. L. & Trotti, A. (October 2010). *AJCC Cancer Staging Manual (7th ed)*, Springer, ISBN 978-0-387-88440-0, New York, NY, USA

el Gammal, S.; Hartwig R.; Aygen S.; Bauermann,T.; Gammal, C. el & Altmeyer, P. (1996). Improved Resolution of Magnetic Resonance Microscopy in Examination of Skin Tumors. *Journal of Investigative Dermatology*, Vol.106, (February 1996), pp. 1287–1292

Essner, R.; Belhocine, T.; Scott, A. M. & Even-Sapir, E. (2006). Novel Imaging Techniques in Melanoma. Surgical Oncology Clinics of North America, Vol.15, No.2, (April 2006), pp. 253–283

Fine, S. & Hansen, W. P. (1971). Optical Second Harmonic Generation in Biological Systems. *Applied Optics*, Vol.10, No.10, (October 1971), pp. 2350–2353

Foster, P. J.; Dunn, E. A.; Karl, K. E.; Snir, J. A.; Nycz, C. M.; Harvey, A. J. & Pettis, R. J. (2008). Cellular Magnetic Resonance Imaging: In Vivo Imaging of Melanoma Cells in Lymph Nodes of Mice. *Neoplasia*, Vol.10, No.3, (March 2008), pp. 207–216

Fujimoto, J. G.; Brezinski, M. E.; Tearney, G. J.; Boppart, S. A.; Bourna, B.; Hee, M. R.; Sourthern, J. F. & Swanson, E. A. (1995). Optical Biopsy and Imaging Using Optical Coherence Tomography. *Nature Medicine*, Vol.1, No.9, (September 1995), pp. 970–972

Gambichler, T.; Moussa, G.; Sand, M.; Sand, D.; Altmeyer, P. & Hoffmann, K. (2005). Applications of Optical Coherence Tomography in Dermatology. *Journal of Dermatological Science*, Vol.40, No.2, (November 2005), pp. 85-94

Gambichler, T.; Matip, R.; Moussa, G.; Altmeyer, P. & Hoffmann, K. (2006). In Vivo Data of Epidermal Thickness Evaluated by Optical Coherence Tomography: Effects of Age, Gender, Skin Type, and Anatomic Site. *Journal of Dermatological Science*, Vol.44, No.3, (December 2006), pp. 145–152

Gambichler, T.; Regeniter, P.; Bechara, F. G.; Orlikov, A.; Vasa, R.; Moussa, G.; Stücker, M.; Altmeyer, P. & Hoffmann, K. (2007). Characterization of Benign and Malignant Melanocytic Skin Lesions Using Optical Coherence Tomography In Vivo. *Journal of the American Academy of Dermatology*, Vol.57, No.4, (October 2007), pp. 629-637

Gareau, D. S.; Merlino, G.; Corless, C.; Kulesz-Martin, M. & Jacques, S. L. (2007). Noninvasive Imaging of Melanoma with Reflectance Mode Confocal Scanning Laser Microscopy in a Murine Model. *Journal of Investigative Dermatology*, Vol.127, (April 2007), pp. 2184–2190

Gareau, D. S.; Patel, Y. G. & Rajadhyaksha, M. (2008). Basic Principles of Reflectance Confocal Microscopy, In: *Reflectance Confocal Microscopy of Cutaneous Tumors*, Gonzalez, S., Gill, M., Halpern, A. C. (Eds.), pp. 1-3, Informa Healthcare, ISBN 0415451043, London, UK

Gerger, A.; Koller, S.; Kern, T.; Massone, C.; Steiger, K.; Richtig, E.; Kerl, H. & Smolle, J. (2005). Diagnostic Applicability of In Vivo Confocal Laser Scanning Microscopy in Melanocytic Skin Tumors. *Journal of Investigative Dermatology*, Vol.124, (March 2005), pp. 493–498

Gerger, A.; Koller, S.; Weger, W.; Richtig, E.; Kerl, H.; Samonigg, H.; Krippl, P. & Smolle, J. (2006). Sensitivity and Specificity of Confocal Laser-Scanning Microscopy for In Vivo Diagnosis of Malignant Skin Tumors. *Cancer*, Vol.107, No.1, (July 2006), pp. 193–200

Gniadecka, M.; Wulf, H. C.; Mortensen, N. N.; Nielsen, O. F. & Christensen, D. H. (1997). Diagnosis of Basal Cell Carcinoma by Raman Spectroscopy. *Journal of Raman Spectroscopy,* Vol.28, (February 1997), pp.125–129

Gniadecka, M.; Wulf, H. C.; Nielsen, O. F.; Christensen, D. H.; Hercogova, J. (1997). Distinctive Molecular Abnormalities in Benign and Malignant Skin Lesions: Studies by Raman Spectroscopy. *Photochem and Photobiol,* Vol.66, No.4, (June 1997), pp. 418–423

Gniadecka, M.; Wulf, H. C.; Nielsen, O. F.; Christensen, D. H.; Hercogova, J. & Rossen, K. (1998). Potential of Raman Spectroscopy for In Vitro and In Vivo Diagnosis of Malignant Melanoma, In: *Proceedings of the XVI International Conference on Raman Spectroscopy.* Heyns, E. M. (Ed.), pp. 764–765, John Wiley and Sons, ISBN 0471983616, Chichester, UK

Gniadecka, M.; Philipsen, P. A.; Sigurdsson, S.; Wessel, S.; Nielsen, O. F.; Christensen, D. H.; Hercogova, J.; Rossen, K.; Thomsen, H. K.; Gniadecki, R.; Hansen, L. K. & Wulf, H. C. (2004). Melanoma Diagnosis by Raman Spectroscopy and Neural Networks: Structure Alterations in Proteins and Lipids in Intact Cancer Tissue. *Journal of Investigative Dermatology,* Vol.122, No.2 (February 2004), pp. 443–449

Gonzalez, S. & Gilaberte-Calzada, Y. (2008). In Vivo Reflectance-Mode Confocal Microscopy in Clinical Dermatology and Cosmetology. *International Journal of Cosmetic Science*, Vol.30, No.1, (February 2008), pp. 1–17

Gritters, L. S.; Francis, I. R.; Zasadny, K. R. & Wahl, R. L. (1993). Initial Assessment of Positron Emission Tomography Using 2-Fluorine- 18-Fluoro-2- Deoxy-D-Glucose in the Imaging of Malignant Melanoma. *Journal of Nuclear Medicine*, Vol. 34, No. 9, (September 1993), pp. 1420-1427

Guitera, P.; Li, L.; Crotty, K.; FitzGerald, P.; Mellenbergh, R.; Pellacani, G. & Menzies, S. (2008). Melanoma Histological Breslow Thickness Predicted by 75-Mhz Ultrasonography. *British Journal of Dermatology*, Vol.159, No.2, (August 2008), pp. 364–369

Häggblad, E.; Petersson, H.; Ilias, M. A.; Anderson, C. D. & Salerud, E. G. (2010). A Diffuse Reflectance Spectroscopic Study of UV-induced Erythematous Reaction across Well-defined Borders in Human Skin. *Skin Research and Technology,* Vol.16, No.3, (August 2010), pp. 283–290

Halton, K. P. (1992). Radiological Considerations in Diagnosis of Metastatic Melanoma: Modern Management of Malignant Melanoma. *The Mount Sinai Journal of Medicine*, Vol.59, No.3, (1992), pp. 211-216, ISSN 0027-2507

Harland, C. C.; Bamber, J. C.; Gusterson, B. A. & Mortimer, P. S. (1993). High Frequency, High Resolution B-Scan Ultrasound in the Assessment of Skin Tumours. *British Journal of Dermatology,* Vol.128, No.5, (May 1993), pp. 525–532

Harland, C. C.; Kale, S.; Jackson, P.; Mortimer, P. S. & Bamber, J. C. (2000), Differentiation of Common Benign Pigmented Skin Lesions from Melanoma by High-Resolution Ultrasound. *British Journal of Dermatology*, Vol.143, No.2, (August 2000), pp. 281–289

Heaston, D. K.; Putman, C. E.; Rodan, B. A.; Nicholson, E.; Ravin, C. E.; Korobkin, M.; Chen, J. T. & Seigler, H. F. (1983). Solitary Pulmonary Metastasis in High Risk Melanoma Patients: a Prospective Comparison of Conventional and Computed Tomography. *American Journal of Roentgenology*, Vol.141, No.1, (1983), pp. 169-174

Hendriks, R. F. M. & Lucassen, G. W. (2000). Two Photon Fluorescence Microscopy of In Vivo Human Skin, *Proceedings of SPIE 2000 Conference on Laser Microscopy, V*ol.4164, pp. 116-121, Amsterdam, Netherlands, July 2000

Henning JS, Dusza SW, Wang SQ, Marghoob, A. A.; Rabinovitz, H. S.; Polsky, D. & Kopf, A. W. (2007). The CASH (Color, Architecture, Symmetry, and Homogeneity) Algorithm for Dermoscopy. *Journal of the American Academy of Dermatology*, Vol.56, No.1, (January 2007), pp. 45-52

Hoffmann, K.; Jung, J.; el Gammal, S. & Altmeyer, P. (1992). Malignant Melanoma in 20-Mhz B Scan Sonography. *Dermatology*, Vol.185, No.1, (1992), pp. 49–55

Holan, S. H. & Viator, J. A. (2008). Automated Wavelet Denoising of Photoacoustic Signals for Circulating Melanoma Cell Detection and Burn Image Reconstruction. *Physics in Medicine and Biology*, Vol.53, No.12, (June 2008), pp. N227–N236

Huang, D.; Swanson, E. A.; Lin, C. P.; Schuman, J. S.; Stinson, W. G.; Chang, W.; Hee, M. R.; Flotte, T.; Gregory, K.; Puliafito, C. A. & Fujimoto, J. G. (1991). Optical Coherence Tomography. *Science*, Vol.254, No.5035, (November 1991), pp. 1178-1181

Hyde, J. S.; Jesmanowicz, A. & Kneeland, J. B. (1987). Surface Coil for MR Imaging of the Skin. *Magnetic Resonance in Medicine*, Vol.5, No.5, (November 1987), pp. 456–461

Iagaru, A.; Quon, A.; Johnson, D.; Gambhir, S. S. & McDougall, I. R. (2006). 2-Deoxy-2-[F-18]fluoro-Dglucose Positron Emission Tomography/Computed Tomography in the Management of Melanoma. *Molecular Imaging and Biology*, Vol.8, No.1, (October 2006), pp. 309-14

Jerant, A. F.; Johnson, J. T.; Sheridan, C. D. & Caffrey T. J. (2000). Early Detection and Treatment of Skin Cancer. *American Family Physician*, Vol.62, No.2, (July 2000), pp. 357-368

Johnson, W. R.; Wilson, D.W.; Fink, W.; Humayun, M. & Bearman, G. (2007). Snapshot Hyperspectral Imaging in Ophthalmology. *Journal of Biomedical Optics*, Vol.12, No.1, (January-February 2007), pp. 0140361-0140367

Kanzler, M. H. & Mraz-Gernhard, S. (2001). Treatment of Primary Cutaneous Melanoma. *Journal of American Medical Association*, Vol.285, No.14, (April 2001), pp. 1819-1821

King, D.M. (2004). Imaging of Metastatic Melanoma. Journal of Hong Kong College of Radiologists, Vol.7, No.2, (2004), pp. 66-69

Kittler, H.; Pehamberger, H.; Wolff, K. & Binder, M. (2002). Diagnostic Accuracy of Dermoscopy. *The LANCET Oncology*, Vol.3, (March 2002), pp. 159-165

König, K. (2000). Laser Tweezers and Multiphoton Microscopes in Life Sciences. *Histochemistry and Cell Biology*, Vol.114, No.2, (July 2000), pp. 79–92

König, K. (2000). Multiphoton Microscopy in Life Sciences. *Journal of Microscopy*, Vol.200, No.2, (November 2000), pp. 83–104

König, K.; Wollina, U.; Riemann, I.; Peuckert, C.; Halbhuber, K. J.; Konrad, H.; Fischer, P.; Fünfstück, V.; Fischer, T. W. & Elsner, P. (2002). Optical Tomography of Human Skin with Subcellular Spatial and Picosecond Time Resolution Using Near Infrared Femtosecond Laser Pulses, *Proceedings of SPIE 2002 Conference on Multiphoton Microscopy in the Biomedical Sciences II*, Vol.4620, pp. 190–201, June 2002

Kopf, A. W.; Elbaum, M. & Provost, N. (1997). The Use of Dermoscopy and Digital Imaging in the Diagnosis of Cutaneous Malignant Melanom*a. Skin Research and Technology*, Vol.3, No.11, (February 1997), pp. 1–7

Langley, R. G.; Burton, E.; Walsh, N.; Propperova, I. & Murray, S. J. (2006). In Vivo Confocal Scanning Laser Microscopy of Benign Lentigines: Comparison to Conventional Histology and In Vivo Characteristics of Lentigo Maligna. *Journal of American Academy of Dermatology*, Vol.55, No.1, (July 2006), pp. 88-97

Lassau, N.; Mercier, S.; Koscielny, S.; Avril, M. F.; Margulis, A.; Mamelle, G.; Duvillard, P. & Leclere, J. (1999). Prognostic Value of High-frequency Sonography and Color Doppler Sonography for the Preoperative Assessment of Melanomas. *American Journal of Roentgenology*, Vol.172, (February 1999), pp. 457–461

Levin, C. S. & Hoffman E. J. (1999). Calculation of Positron Range and Its Effect on the Fundamental Limit of Positron Emission Tomography System Spatial Resolution. *Physics in Medicine and Biology*, Vol.44, No.3, (March 1999), pp. 781-799

Li, B.; Majaron, B.; Viator, J. A.; Milner, T. E.; Chen, Z.; Zhao, Y.; Ren, H. & Nelson, J. S. (2004). Accurate Measurement of Blood Vessel Depth in Port Wine Stained Human Skin In Vivo Using Pulsed Photothermal Radiometry. *Journal of Biomedical Optics*, Vol.9, No.5, (September-October 2004), pp. 961-966

Lim, R. S.; Kratzer, A.; Barry, N. P.; Miyazaki-Anzai, S.; Miyazaki, M.; Mantulin, W. W.; Levi, M.; Potma, E. O. & Tromberg, B. J. (2010). Multimodal CARS Microscopy Determination of the Impact of Diet on Macrophage Infiltration and Lipid Accumulation on Plaque Formation in ApoE-deficient Mice. *Journal of Lipid Research*, Vol.51, No.7, (July 2010), pp. 1729-37

Link, T. M.; Vieth V.; Stehling, C.; Lotter, A.; Beer, A.; Newitt, D. & Majumdar, S. (2002). High-Resolution MRI vs Multislice Spiral CT: Which Technique Depicts the Trabecular Bone Structure Best?. *European Radiology*, Vol.13, No.4, (September 2002), pp. 663-671

Lohela, M. & Werb, Z. (2010). Intravital Imaging of Stromal Cell Dynamics in Tumors. *Current Opinion in Genetics and Development*, Vol.20, No.1, (February 2010), pp. 72-78

Macfarlane, D. J.; Sondak, V.; Johnson, T. & Wahl, R. L. (1998). Prospective Evaluation of 2-(18F)-2-deoxyglucose Positron Emission Tomography in Staging of Regional Lymph Nodes in Patients with Cutaneous Malignant Melanoma. *Journal of Clinical Oncology*, Vol.16, No.5, (May 1998), pp. 1770-1776

Machet, L.; Belot, V.; Naouri, M.; Boka, M.; Mourtada, Y.; Giraudeau, B.; Laure, B.; Perrinaud, A.; Machet, M. & Vaillant, L. (2009). Preoperative Measurement of Thickness of Cutaneous Melanoma Using High-Resolution 20 MHz Ultrasound Imaging: A Monocenter Prospective Study and Systematic Review of the Literature, *Ultrasound in Medicine and Biology*, Vol.35, No.9, (September 2009), pp. 1411-1420

MacKie, R. M. (1971). An Aid to the Preoperative Assessment of Pigmented Lesions of the Skin. *British Journal of Dermatology*, Vol.85, No.3, (September 1971), pp. 232-238

Mansfield, J. R.; Hoyt, C. C.; Miller, P. J. & Levenson, R. M. (2005). Distinguished Photons: Increased Contrast with Multispectral In Vivo Fluorescence Imaging. *Biotechniques*, Vol.39, (December 2005), pp. S33–S37

Marchesini, R.; Brambilla, M.; Clemente, C.; Maniezzo, M.; Sichirollo, A. E.; Testori, A.; Venturoli, D. R. & Cascinelli, N. (1991). In Vivo Spectrophotometric Evaluation of Neoplastic and Non-Neoplastic Skin Pigmented Lesions–I. Reflectance Measurements. *Photochemistry and Photobiology*, Vol.53, No.1, (January 1991), pp. 77–84

Marchesini, R.; Cascinelli, N.; Brambilla, M.; Clemente, C.; Mascheroni, L.; Pignoli, E.; Testori, A. & Venturoli, D. R. (1992). In Vivo Spectrophotometric Evaluation of Neoplastic and Non-Neoplastic Skin Pigmented Lesions. II: Discriminant Analysis between Nevus and Melanoma. *Photochemistry and Photobiology*, Vol.55, No.4, (April 1992), pp. 515–522

Marchesini, R.; Bono, A.; Tomatis, S.; Bartoli, C.; Colombo, A.; Lualdi, M. & Carrara, M. (2007). In Vivo Evaluation of Melanoma Thickness by Multispectral Imaging and an Artificial Neural Network. A Retrospective Study on 250 Cases of Cutaneous Melanoma. *Tumori,* Vol.93, No.2, (March-April 2007), pp. 170-177

Marghoob, A. A.; Swindle, L. D.; Moricz, C. Z. M. S.; Sanchez-Negron, F. A.; Slueb, B.; Halpern, A. C. & Kopf, A. W. (2003). Instruments and New Technologies for the In Vivo Diagnosis of Melanoma. *Journal of the American Academy of Dermatology*, Vol.49, No.5, (November 2003), pp. 777-797

Marghoob, A. A. & Halpern, A. C. (2005). Confocal Scanning Laser Reflectance Microscopy: Why Bother?. *Archives of Dermatology*, Vol.141, No.2, (February 2005), pp. 212-215

Maslov, K.; Stoica, G. & Wang, L. V. (2005). In Vivo Dark-Field Reflectionmode Photoacoustic Microscopy. *Optics Letters*, Vol.30, No.6, (March 2005), pp. 625-627

Masters, B. R.; So, P. T. C. & Gratton, E. (1997). Multiphoton Excitation Fluorescence Microscopy and Spectroscopy of In Vivo Human Skin. *Biophysical Journal*, Vol.2, No.6, (June 1997), pp. 2405-2412

Masters, B. R.; So, P. T. C. & Gratton, E. (1998). Multiphoton Excitation Microscopy of In Vivo Human Skin, In: *Advances in Optical Biopsy and Optical Mammography*, Alfano, R. R. (Ed.), Vol.838, pp. 58–67, New York Academy of Sciences, New York, NY, USA

Meyer, L. E.; Otberg, N.; Sterry, W. & Lademann, J. (2006). In Vivo Confocal Scanning Laser Microscopy: Comparison of the Reflectance and Fluorescence Mode by Imaging Human Skin. *Journal of Biomedical Optics*, Vol.11, No.4, (August 2006), pp. 11–17

Mihm, M. C.; Murphy, G. F. & Kaufman, N. (1988). *Pathobiology and Recognition of Malignant Melanoma*, United States and Canadian Academy of Pathology, New York, NY, USA

Milanič, M.; Majaron B. & Nelson, J. S. (2007). Pulsed Photothermal Temperature Profiling of Agar Tissue Phantoms, *Lasers in Medical Science*, Vol.22, No.4, (May 2007), pp. 279-284

Milner, T. E.; Smithies, D. J.; Goodman, D. M.; Lau, A. & Nelson, J. S. (1996). Depth Determination of Chromophores in Human Skin by Pulsed Photothermal Radiometry. *Applied Optics*, Vol.35, No.19, (June 1996), pp. 3379-3385

Moreaux, L.; Sandre, O. & Mertz, J. (2000). Membrane Imaging by Second-harmonic Generation Microscopy. *Journal of the Optical Society of America B: Optical Physics*, Vol.17, No.10, (October 2000), pp. 1685-1694

Nehal, K. S.; Gareau, D. & Rajadhyaksha, M. (2008). Skin Imaging with Reflectance Confocal Microscopy. *Seminars in Cutaneous Medicine and Surgery*, Vol.27, No.1, (March 2008), pp. 37-43

Nijssen, A., Bakker Schut, T. C.; Heule, F.; Caspers, P. J.; Hayes, D. P.; Neumann, M. H. A. & Puppels, G. J. (2002). Discriminating Basal Cell Carcinoma from Its Surrounding Tissue by Raman Spectroscopy. *Journal* of *Investigative Dermatology,* Vol.119, No.1, (July 2002), pp. 64–69

Oh, J.; Li, M.; Zhang, H. F.; Maslov, K. & Wang, L. V. (2006). Three-dimensional Imaging of Skin Melanoma In Vivo by Dual-Wavelength Photoacoustic Microscopy. *Journal of Biomedical Optics*, Vol.11, No.3, (June 2006), pp. 0340321-0340324

Olmedo, J. M.; Warschaw, K. E.; Schmitt, J. M. & Swanson, D. L. (2006). Optical Coherence Tomography for the Characterization of Basal Cell Carcinoma In Vivo: a Pilot Study. *Journal of the American Academy of Dermatology*, Vol.55, No.3, (September 2006), pp. 408-412

Ono, I. & Kaneko, F. (1995), Magnetic Resonance Imaging for Diagnosing Skin Tumors. *Clinics in Dermatology*, Vol.13, No.4, (July-August 1995), pp. 393-399

Passmann, C. & Ermert, H. (1999). A 100-MHz Ultrasound Imaging System for Dermatologic and Ophthalmologic Diagnostics. *IEEE Transactions on Ultrasonics, Ferroelectrics, and Frequency Control*, Vol.43, No.4, (July 1999), pp. 545-552

Pavlin, C. J.; Sherar, M. D. & Foster, F. S. (1990). Subsurface Ultrasound Microscopic Imaging of the Intact Eye. *Ophthalmology,* Vol.97, No.2, (February 1990), pp. 244-250

Pellacani, G.; Cesinaro, A. M. & Seidenari, S. (2005). Reflectance-mode Confocal Microscopy of Pigmented Skin Lesions-Improvement in Melanoma Diagnostic Specificity. *Journal of the American Academy of Dermatology*, Vol.53, No.6, (December 2005), pp. 979-985

Pellacani, G.; Guitera, P.; Longo, C.; Avramidis, M.; Seidenari, S. & Menzies, S. (2007). The Impact of In Vivo Reflectance Confocal Microscopy for the Diagnostic Accuracy of Melanoma and Equivocal Melanocytic Lesions. *Journal of Investigative Dermatology*, Vol.127, (July 2007), pp. 2759-2765

Peuckert, C.; Riemann, I. & König, K. (2000). Two Photon Induced Autofluorescence of In Vivo Human Skin with Femtosecond Laser Pulses-a Novel Imaging Tool of High Spatial, Spectral and Temporal Resolution. *Cellular and Molecular Biology*, Vol.46, (2000), abstract 179

Pfannenberg, C.; Aschoff, P.; Schanz, S.; Eschmann, S. M.; Plathow, C.; Eigentler, T. K.; Garbe, C.; Brechtel, K.; Vonthein, R.; Bares, R.; Claussen C. D. & Schlemmer, H. P. (2007). Prospective Comparison of ^{18}F-fluorodeoxyglucose Positron Emission

Tomography/Computed Tomography and Whole-body Magnetic Resonance Imaging in Staging of Advanced Malignant Melanoma. *European Journal of Cancer*, Vol.43, No.3, (February 2007), pp. 557-564

Querleux, B. (1995). Nuclear Magnetic Resonance (NMR) Examination of the Epidermis In Vivo, In: *Handbook of Non-Invasive Methods and the Skin*, Serup, J. & Jemec, G. B. E. (Eds.), pp. 133–139, CRC, ISBN 0849314372, Boca Raton, FL, USA

Querleux, B.; Yassine, M. M.; Darrasse, L.; Saint-Jalmes, H.; Sauzade, M. & Leveque, J. L. (1988). Magnetic Resonance Imaging of the Skin. A Comparison with the Ultrasonic Technique. *Bioengineering and the Skin*, Vol.4, No.1, (1988), pp. 1–14, ISSN 0266-3082

Rajadhyaksha, M.; Grossman, M.; Esterowitz, D.; Webb, R. H. & Anderson, R. R. (1995). In Vivo Confocal Scanning Laser Microscopy of Human Skin: Melanin Provides Strong Contrast. *Journal of Investigative Dermatology*, Vol.104, No.6, (June 1995), pp. 946–952

Rajeswari, M. R.; Jain, A; Sharma, A.; Singh, D.; Jagannathan, N. R.; Sharma, U. & Degaonkar, M. N. (2003). Evaluation of Skin Tumors by Magnetic Resonance Imaging. *Laboratory Investigation*, Vol.83, (May 2003), pp. 1279–1283

Reinhardt, M. J.; Joe, A. Y.; Jaeger, U.; Huber, A.; Matthies, A.; Bucerius, J.; Roedel, R.; Strunk, H.; Bieber, T.; Biersack, H. & Tüting T. Diagnostic Performance of Whole Body Dual Modality 18F-FDG PET/CT Imaging for N- and M-Staging of Malignant Melanoma: Experience with 250 Consecutive Patients. *Journal of Clinical Oncology*, Vol.24, No.7, (March 2006), pp. 1178-1187

Richard, S.; Querleux, B.; Bittoun, J.; Idy-Peretti, I.; Jolivet, O.; Cermakowa, E. & Leveque, J. L. (1991). In Vivo Proton Relaxation Times Analysis of Skin Layers by Magnetic Resonance Imaging. *Journal of Investigative Dermatology*, Vol.97, (February 1991), pp. 120–125

Ries, L.; Eisner, M.; Kosary, C.; Hankey, B.; Miller, B. & Clegg, L. (2003). SEER Cancer Statistics Review, 1975-2000. *National Cancer Institute*, (2003), Tables XV1-9

Rinne, D.; Baum, R.P.; Hor, G. & Kaufmann, R. (1998). Primary Staging and Followup of High Risk Melanoma Patients with Whole Body 18 F-fluorodeoxyglucose Positron Emission Tomography: Results of a Prospective Study of 100 Patients. *Cancer*, Vol.82, No.9, (1998), pp. 1664-1671, ISSN 0008-543X

Roth, S. & Freund, I. (1979). Second Harmonic-Generation in Collagen. *Journal of Chemical Physics*, Vol.70, No.4, (February 1979), pp. 1637–1643

Rubin, K. M. (2010). Melanoma Staging: A Review of the Revised American Joint Committee on Cancer Guidelines. Journal of the Dermatology Nurses' Association, Vol.2, No.6, (November-December 2010), pp. 254-259

Schenk, J. O. & Brezinski, M. E. (2002). Ultrasound Induced Improvement in Optical Coherence Tomography (OCT) Resolution. *Proceedings of the National Academy of Sciences of the United States of America*, Vol.99, No.15, (July 2002), pp. 9761-9764

Schick, F. (2005). Whole-Body MRI at High Field: Technical Limits and Clinical Potential. *European Radiology*, Vol.31, No.5, (May 2005), pp. 946–959

Schroeder, S.; Kopp, A. F.; Baumbach, A.; Meisner, C.; Kuettner, A.; Georg, C.; Ohnesorge, B.; Herdeg, C.; Claussen, C. D. & Karsch, K. R. (2001). Noninvasive Detection and Evaluation of Atherosclerotic Coronary Plaques with Multislice Computed Tomography. *Journal of the American College of Cardiology*, Vol.37, No.5, (April 2001), pp. 1430-1435

Serrone, L.; Solivetti, F. M.; Thorel, M. F.; Eibenschutz, L.; Donati, P. & Catricala, C. (2002). High Frequency Ultrasound in the Preoperative Staging of Primary Melanoma: a Statistical Analysis. *Melanoma Research*, Vol.12, No.3, (June 2002), pp. 287–290

Shi, J.; Zheng,Y. P.; Chen, X. & Huang, Q. H. (2007). Assessment of Muscle Fatigue Using Sonomyography: Muscle Thickness Change Detected from Ultrasound Images. *Medical Engineering and Physics*, Vol.29, No.4, (May 2007), pp. 472-479

Sladden, M. J.; Balch, C.; Barzilai, D. A.; Berg, D.; Freiman, A.; Handiside, T.; Hollis, S.; Lens, M. B. & Thompson, J. F. (2009). Surgical Excision Margins for Primary Cutaneous Melanoma. *Cochrane Database of Systematic Reviews*, No.4, (October 2009), pp. 1-34

Smith, L. & MacNeil, S. (2011), State of the Art in Non-Invasive Imaging of Cutaneous Melanoma. *Skin Research and Technology*, Vol.17, (February 2011), doi: 10.1111/j.1600-0846.2011.00503.x

So, P. T. C. & Kim, H. (1998). Two-photon Deep Tissue Ex Vivo Imaging of Mouse Dermal and Subcutaneous Structures. *Optics Express*, Vol.3, No.9, (October 1998), pp. 339–350

Song, K. H.; Kim, C.; Maslov, K. & Wang, L. V. (2009). Noninvasive In Vivo Spectroscopic Nanorod-Contrast Photoacoustic Mapping of Sentinel Lymph Nodes. *European Journal of Radiology*, Vol.70, No.2, (May 2009), pp. 227-231

Steinert, H. C.; Huch Böni, R. A.; Buck, A.; Böni, R.; Berthold, T.; Marincek, B.; Burg, G. & von Schulthess, G. K. (1995). Malignant Melanoma: Staging with Whole Body Positron Emission Tomography and 2-(F-18)-fluoro-2-deoxy-D-glucose. *Radiology*, Vol.195, (June 1995), pp. 705-709

Strobel, K.; Dummer, R.; Husarik, D. B.; Lago, M. P.; Hany, T. F. & Steinert, H. C. (2007). High-Risk Melanoma: Accuracy of FDG PET/CT with Added CT Morphologic Information for Detection of Metastases. *Radiology*, Vol.244, No.2, (August 2007), pp. 566-574

Sun, T. & Diebold, G. J. (1992). Generation of Ultrasonic Waves from a Layered Photoacoustic Source. *Nature*, Vol.355, (February 1992), pp. 806–808

Tacke, J.; Haagen, G.; Hornstein, O. P.; Huettinger, G.; Kiesewetter, F.; Schell, H. & Diepgen, T. L. (1995). Clinical Relevance of Sonometry-derived Tumour Thickness in Malignant Melanoma: a Statistical Analysis. *British Journal of Dermatology*, Vol.132, No.2, (February 1995), pp. 209–214

Tannous, Z. S.; Lerner, L. H.; Duncan, L. M.; Mihm Jr, M. C. & Flotte, T. J. (2000). Progression to Invasive Melanoma from Malignant Melanoma In Situ, Lentigo Maligna Type. *Human Pathology*, Vol.31, No.6, (June 2000), pp. 705-708

Tannous, Z. S.; Mihm, M. C.; Flotte, T. J. & Gonzalez, S. (2002). In Vivo Examination of Lentigo Maligna and Malignant Melanoma In Situ, Lentigo Maligna Type by Near-Infrared Reflectance Confocal Microscopy: Comparison of In Vivo Confocal Images with Histologic Sections. *Journal of American Academy of Dermatology*, Vol.46, No.2, (February 2002), pp. 260-263

Teuchner, K.; Freyer, W.; Leupold, D.; Volkmer, A.; Birch, D. J. S.; Altmeyer, P.; Stucker, M. & Hoffmann, K. (1999). Femtosecond Two-photon Excited Fluorescence of Melanin. *Photochemistry and Photobiology*, Vol.70, No.2, (August 1999), pp. 146–151

Theodossiou, T. A.; Thrasivoulou, C.; Ekwobi, C. & Becker, D. L. (2006). Second Harmonic Generation Confocal Microscopy of Collagen Type I from Rat Tendon Cryosections. *Biophysical Journal*, Vol.91, No.12, (December 2006), pp. 4665-4677

Thrasivoulou, C.; Virich, G.; Krenacs, T.; Korom, I. & Becker, D. L. (2011). Optical Delineation of Human Malignant Melanoma Using Second Harmonic Imaging of Collagen. *Biomedical Optics Express*, Vol.2, No.5, (May 2011), pp. 1282-1295

Totty, W. G.; Murphy, W. A. & Lee, J. K. T. (1986). Soft-tissue Tumors: MR Imaging. *Radiology*, Vol.160, (July 1986), 135-141.

Tripp, J. M.; Kopf, A. W.; Marghoob, A. A. & Bart, R. S. (2002). Management of Dysplastic Nevi: a Survey of Fellows of the American Academy of Dermatology. *Journal of the American Academy of Dermatology*, Vol.46, No.5, (May 2002), pp. 674-682

Tuzcu, E. M.; Bayturan, O. & Kapadia, S. (2010). Coronary Intravascular Ultrasound: a Closer View. *Heart*, Vol.96, No.16, (2010), pp. 1318-1324

Ulrich, J.; Petereit, S. & Gollnick, H. (1999). The Preoperative Diagnostics of Malignant Melanoma - Comparison of 7.5-MHz- and 20-MHz-Sonography. *Ultraschall in Medicine*, Vol.20, No.5, (1999), pp. 197-200

Wagner, J. D.; Schauwecker, D.; Hutchins, G. & Coleman, J. J. (1997). Initial Assessment of Positron Emission Tomography for Detection of Nonpalpable Regional Lymphatic Metastases in Melanoma. *Journal of Surgical Oncology*, Vol.64, No.3, (March 1997), pp. 181–189

Wagner, J. D.; Schauwecker, D.; Davidson, D.; Coleman III, J. J.; Saxman, S.; Hutchins, G.; Love, C. & Hayes, J. T. (1999). Prospective Study of Fluorodeoxyglucose–Positron Emission Tomography Imaging of Lymph Node Basins in Melanoma Patients Undergoing Sentinel Node Biopsy. *Journal of Clinical Oncology*, Vol. 17, No. 5, (May 1999), 1508-1515

Wallace, V. P.; Crawford, D. C.; Mortimer, P. S.; Ott, R. J. & Bamber, J. C. (2000). Spectrophotometric Assessment of Pigmented Skin Lesions: Methods and Feature Selection for Evaluation of Diagnostic Performance. *Physics in Medicine and Biology,* Vol.45, No.3, (January 2000), pp. 735–751

Wallace, V. P.; Bamber, J. C.; Crawford, D. C.; Ott, R. J. & Mortimer P. S. (2000). Classification of Reflectance Spectra from Pigmented Skin Lesions, a Comparison of Multivariate Discriminant Analysis and Artificial Neural Networks. *Physics in Medicine and Biology,* Vol.45, No.10, (March 2000), pp. 2859-2871.

Wang, H.; Huff, T. B.; Zweifel, D. A.; He, W.; Low, P. S.; Wei, A. & Cheng, J. (2005). In Vitro and In Vivo Two-photon Luminescence Imaging of Single Gold Nanorods. *Proceedings of the National Academy of Sciences of the United States of America*, Vol.102, No.44, (November 2005), pp. 15752-15756

Wang, H.; Langohr, I. M.; Sturek M. & Cheng, J. (2009). Imaging and Quantitative Analysis of Atherosclerotic Lesions by CARS-Based Multimodal Nonlinear Optical Microscopy. *Arteriosclerosis, Thrombosis, and Vascular Biology,* Vol.29, (June 2009), pp. 1342-1348

Wang, T.; Qiu, J.; Paranjape, A. S. & Milner, T. E. (2009). Melanoma Thickness Measurement in Two-layer Tissue Phantoms Using Pulsed Photothermal Radiometry (PPTR), *Proceedings of SPIE 2009 Conference on Optical Interactions with Tissue and Cells XX*, Vol.7175, pp. 71750L1-71750L9, San Jose, CA, USA, January 2009

Wang, T.; Mallidi, S.; Qiu, J.; Ma, L. L.; Paranjape, A. S.; Sun, J.; Kuranov, R. V.; Johnston, K. P. & Milner, T. E. (2011). Comparison of Pulsed Photothermal Radiometry, Optical Coherence Tomography and Ultrasound for Melanoma Thickness Measurement in PDMS Tissue Phantoms. *Journal of Biophotonics*, Vol.4, No.5, (May 2011), pp. 335–344

Wang, X.; Pang, Y.; Ku, G.; Xie, X.; Stoica, G. & Wang, L. V. (2003). Noninvasive Laser-Induced Photoacoustic Tomography for Structural and Functional In Vivo Imaging of the Brain. *Nature Biotechnology*, Vol.21, (June 2003), pp. 803-806

Weber, J. R.; Cuccia, D. J.; Johnson, W. R.; Bearman, G. H.; Durkin, A. J.; Hsu, M.; Lin, A.; Binder, D. K.; Wilson D. & Tromberg, B. J. (2011). Multispectral Imaging of Tissue Absorption and Scattering Using Spatial Frequency Domain Imaging and a Computed-Tomography Imaging Spectrometer. *Journal of Biomedical Optics*, Vol.16, No.1, (January 2011), pp. 0110151-0110157

Weeks, R. G.; Berquist, T. H.; McLeod, R. A. & Zimmer, W. D. (1985). Magnetic Resonance Imaging of Soft-Tissue Tumors: Comparison with Computed Tomography. *Magnetic Resonance Imaging*, Vol.3, No.4, (September 1985), pp. 345-352

Weight, R. M.; Viator, J. A.; Dale, P. S.; Caldwell, C. W. & Lisle, A. E. (2006). Photoacoustic Detection of Metastatic Melanoma Cells in the Human Circulatory System. *Optics Letters*, Vol.31, No.20, (October 2006), pp. 2998–3000

Welzel, J. (2001). Optical Coherence Tomography in Dermatology: a Review. *Skin Research and Technology*, Vol.7, No.1, (February 2001), pp. 1–9

Welzel, J.; Bruhns, M. & Wolff, H. H. (2003). Optical Coherence Tomography in Contact Dermatitis and Psoriasis. *Archives of Dermatological Research*, Vol.295, No.2, (April 2003), pp. 50-55

Yao, W. J.; Hoh, C.K. & Glaspy, F. (1994). Whole Body FDG-PET Imaging for Staging Of Malignant Melanoma: Is It Cost Effective?. *Journal of Nuclear Medicine*, Vol.35, (May 1994), pp. 8P, ISSN 0161-5505

Zemtsov, A.; Lorig, R.; Bergfield, W. F.; Bailin, P. L. & Ng, T. C. (1989). Magnetic Resonance Imaging of Cutaneous Melanocytic Lesions. *Journal of Dermatologic Surgery and Oncology*, Vol.15, No.8, (August 1989), pp. 854-858

Zhang, H. F.; Maslov, K.; Stoica, G. & Wang, L. V. (2006). Functional Photoacoustic Microscopy for High-Resolution and Noninvasive In Vivo Imaging. *Nature Biotechnology*, Vol.24, (June 2006), pp. 848 - 851

Zharov, V. P.; Galanzha, E. I.; Shashkov, E. V.; Khlebtsov, N. G. & Tuchin, V. V. (2006). In Vivo Photoacoustic Flow Cytometry for Monitoring of Circulating Single Cancer Cells and Contrast Agents. *Optics Letters*, Vol.31, No.24, (December 2006), pp. 3623–3625

Zipfel, W. R.; Williams, R. M.; Christie, R.; Nikitin, A. Y.; Hyman, B. T. & Webb, W. W. (2003). Live Tissue Intrinsic Emission Microscopy Using Multiphotonexcited Native Fluorescence and Second Harmonic Generation. *Proceedings of the National Academy of Sciences of the United States of America*, Vol.100, No.12, (June 2003), pp. 7075–7080

Zipfel, W. R.; Williams, R. M. & Webb, W. W. (2003). Nonlinear Magic: Multiphoton Microscopy in the Biosciences. *Nature Biotechnology*, Vol.21, No.11, (November 2003), pp. 1369 –1377
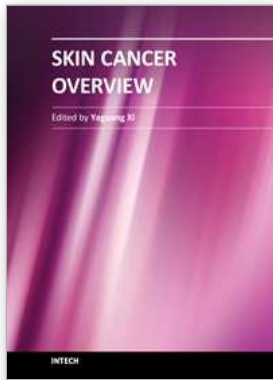
Skin Cancer Overview

Edited by Dr. Yaguang Xi

The book Skin Cancer Overview is divided into three sections to cover the most essential topics in skin cancer research: Etiology, Diagnosis and Treatment, and Prevention. Due to the complexity of skin cancer, this book attempts to not only provide the basic knowledge, but also present the novel trends of skin cancer research. All chapters were written by experts from around the world. It will be a good handbook for researchers with interests in skin cancer.

How to reference

In order to correctly reference this scholarly work, feel free to copy and paste the following:

Tianyi Wang, Jinze Qiu and Thomas E. Milner (2011). Determination of Melanoma Lateral and Depth Margins: Potential for Treatment Planning and Five-Year Survival Rate, Skin Cancer Overview, Dr. Yaguang Xi (Ed.), ISBN: 978-953-307-746-8, InTech, Available from: http://www.intechopen.com/books/skin-cancer-overview/determination-of-melanoma-lateral-and-depth-margins-potential-for-treatment-planning-and-five-year-s

INTECH
open science | open minds